UNIVERSITY OF CALIFORNIA,
IRVINE

Psychophysical Inference from Centroid Estimation

DISSERTATION

submitted in partial satisfaction of the requirements
for the degree of

DOCTOR OF PHILOSOPHY

in Cognitive Sciences

by

Jordan Ali Rashid

Dissertation Committee:
Professor Charles Chubb, Chair
Professor Barbara Dosher
Professor Michael Dzmura

2019

DEDICATION

For anyone who sees geometry in the vibration of strings, or hears music in the motion of spheres...

TABLE OF CONTENTS

LIST OF FIGURES

LIST OF TABLES

ACKNOWLEDGMENTS

I would like to thank my mother,

Geraldine Seigler for teaching me to see things I could not measure,

Anne Sutter for teaching me to measure things I could not see,

Geoffrey Iverson for teaching me to capture uncertainty,

and Charles Chubb for teaching me to celebrate it.

CURRICULUM VITAE

Jordan Ali Rashid

EDUCATION

Doctor of Philosophy in Cognitive Sciences **2019**
University of California *Irvine, California*

Master of Arts in Psychology **2016**
University of California *Irvine, California*

Bachelor of Science in Psychology **2013**
Loyola University *Chicago, Illinois*

RESEARCH EXPERIENCE

Graduate Research Assistant **2014–2019**
University of California *Irvine, California*

Research Assistant at Sanocki Laboratory **2013–2014**
University of South Florida *Tampa, Florida*

Research Assistant at Sutter Laboratory **2009–2013**
University of Loyola *Chicago, Illinois*

Research Assistant at Dye Laboratory **2010–2012**
University of Loyola *Chicago, Illinois*

TEACHING EXPERIENCE

Teaching Assistant **2014–2019**
University of California *Irvine, California*

Teaching Assistant **2004–2008**
Academy Prep of Tampa *Tampa, Florida*

REFEREED JOURNAL PUBLICATIONS

REFEREED CONFERENCE PUBLICATIONS

Two Centroid Mechanisms in Vision **May 2015**
Vision Sciences Society

The Density Effect in Centroid Estimation **May 2016**
Vision Sciences Society

Centroid Estimates are Influenced by Prior Beliefs **May 2017**
Vision Sciences Society

ABSTRACT OF THE DISSERTATION

Psychophysical Inference from Centroid Estimation

By

Jordan Ali Rashid

Doctor of Philosophy in Cognitive Sciences

University of California, Irvine, 2019

Professor Charles Chubb, Chair

Performance statistics in centroid tasks are not the same as those used in classic decision tasks. In psychophysical experiments using decision tasks, signal detection theory and drift-diffusion models provide the frameworks for statistical inference from error rates and reaction times. However, neither of these frameworks are appropriate for psychophysical inference with centroid task data. In this dissertation, we explore a modeling framework for double-pass experiments with centroid tasks, and show its potential to (1) detect performance differences, and infer experimental effects without additional process model assumptions, (2) falsify properties of a latent process using nested model assumptions, (3) investigate neurocomputational models of the process, and (4) investigate properties of spatial attention at a deeper level than is possible using decision-based paradigms.

Chapter 1

Estimation strategies and psychophysical inference

1.1 Strategic estimator modeling framework

Like the application of signal detection theory in psychophysics, the strategic estimator modeling framework should generalize to many psychophysical tasks. The current version is designed to enable psychophysical inference from experimental data collected under conditions with the following properties:

1. In a type I task (Sperling, 2008), subjects are instructed to report their estimates of a latent interval variable.
2. Performance statistics follow a distribution of quadratic sums (i.e. sum-of-squares).
3. Subjects are trained with feedback until performance saturates at some performance criterion.
4. A double-pass procedure is used in experimental sessions.

A *strategy* is a method of anticipating feedback based on an information summary made available by the stimulus. Developing a strategy means learning which *mechanisms* are effective predictors of the stimulus-conditioned feedback, and a *target estimator* (i.e. a representation of the target location available from the mechanisms). The *effectiveness* of a mechanism is task-dependent property of the mechanism's response to the stimulus. Quantitatively, it is the reduction in spatial uncertainty over target locations given knowledge of the response. In other words, the most effective mechanisms provide the largest constraints on possible target locations.

Some other defining characteristics of a strategy are:

1. Strategies emerge from some mental process involving learning, memory, and conscious effort, and are expected to increase/decrease the reward/cost of behavior.

2. Strategies require an understanding of the task instructions, and conditions where task is typically performed.

3. Strategy development is driven by changes in effectiveness, which are detectable in the reward prediction error signals following feedback.

4. Strategies are prescribed ahead of time, so the most effective mechanisms can be deployed rapidly with little-to-no conscious effort.

1.2 What is a strategic estimator?

A strategic estimator is a function that maps stimulus patterns onto a perceptual representation of the target location (i.e the expected response location). Just like any other estimator in Estimation Theory, strategic estimators can be compared objectively in terms

of the *mean-squared error* parameters (Casella and Berger, 2002). These performance statistics follow distributions of quadratic sums, which have been studied previously (Fraser et al., 1951; Solomon, 1953; Fraser, 1953; Grad and Solomon, 1955; Harter, 1960; Solomon et al., 1961; Bock and Solomon, 1988) (see (Washburn et al., 2009) for a thorough review).

1.2.1 Quantitative definitions

1.2.1.1 Preliminaries

We write vectors bold text (ex: $\mathbf{R}$ or $\boldsymbol{\beta}$).

We write $\left\| \cdot \right\|$ for the 2-norm operator (i.e. Euclidean distance).

We write $\mathrm{E}\left[\ \cdot \ \right]$ for the expectation operator, and $\mathrm{E}\left[X \mid Y\right]$ for the expectation of X given Y (i.e. conditional expectations).

We write S for a stimulus (i.e. any set of item locations and features).

We write $\mathbf{T}(S)$ for the target of S.

We write $\mathbf{R}(S)$ for the response of a subject after presentation of S.

We write $\boldsymbol{\phi}(S)$ for the strategic estimator applied to stimulus S.

1.2.1.2 New quantities

Equation 1.1 defines strategic estimators in terms of predicted responses to the stimulus pattern S.

$$\boldsymbol{\phi}(S) = \mathrm{E}\big[\ \mathbf{R}\ \big|\ S\ \big] \tag{1.1}$$

$$2\sigma^2 = \mathrm{E}\big[\ \big\|\mathbf{R} - \boldsymbol{\phi}\big\|^2\ \big] \tag{1.2}$$

Equation 1.3 defines the likelihood model in terms of these parameters.

$$\mathbf{R}(S)\ \sim\ \mathrm{Normal}\big(\ \boldsymbol{\phi}(S)\ ,\ \sigma^2 I\ \big) \tag{1.3}$$

The *bias* of a strategic estimator given the stimulus S is defined in equation 1.4.

$$\begin{aligned}\boldsymbol{\beta}(S) &= \mathrm{E}\big[\ \mathbf{R} - \mathbf{T}\ \big|\ S\ \big] \\ &= \boldsymbol{\phi}(S) - \mathbf{T}(S)\end{aligned} \tag{1.4}$$

The *mean-squared error* of a strategic estimator given the stimulus S is defined in equation 1.5.

$$\begin{aligned}\gamma(S) &= \mathrm{E}\big[\ \big\|\mathbf{R} - \mathbf{T}\big\|^2\ \big|\ S\ \big] \\ &= \big\|\boldsymbol{\beta}(S)\big\|^2 + 2\sigma^2\end{aligned} \tag{1.5}$$

An important property of the decomposition in equation 1.5 is that the two terms in the second line make statistically independent contributions to inferences about γ (Cochran, 1934).

1.3 Double-pass methods

Applications of signal detection theory based on normal models of latent decision variables pool all sources of variability into a single additive noise term. The framework is suitable for inferring parameters of a binary classifier from estimates of the hit and false alarm rates from psychophysical data. More recently, using the using classic paradigms, diffusion modeling of reaction times have allowed for richer descriptions of the perceptual and cognitive mechanisms mediating the relationship(s) between stimuli and responses. For example, Ratcliff et al. (2018) used diffusion modeling in a series of double-pass experiments to show variability should not be explained by a single noise term. The authors argue that total response variability should be partitioned into random, systematic, and stimulus-dependent terms, which jointly explain patterns in hit rates, false alarm rates, and reaction times. Inference with the strategic estimator modeling framework proceeds somewhat differently because performance is operationally defined in terms of mean-squared distance (eq. 1.5), and uses the decomposition rule to partition total response error into systematic bias (eq. 1.4) and random error (eq. 1.2).

1.3.1 Quantitative definitions

The double-pass method provides unbiased estimators for the quantities in equations 1.1, 1.2, 1.4, and 1.5.

1.3.1.1 Preliminaries

If $S_1, S_2, \cdots, S_K$ (i.e. a sequence of K stimuli) is presented to a subject under identical conditions, we refer to the k-th stimulus in the sequence as S_k.

We write $\mathbf{R}_1(S_k)$ and $\mathbf{R}_2(S_k)$ to denote the response observed after the first and second presentation of stimulus S_k.

1.3.1.2 New quantities

We begin with an unbiased estimator of $\boldsymbol{\phi}(S_k)$, obtained from the pair of bivariate responses, $\mathbf{R}_1(S_k)$ and $\mathbf{R}_2(S_k)$:

$$\hat{\boldsymbol{\phi}}_k = \frac{1}{2}\left[\mathbf{R}_1(S_k) + \mathbf{R}_2(S_k) \right] \tag{1.6}$$

Of all unbiased estimators for $\boldsymbol{\phi}(S_k)$, $\hat{\boldsymbol{\phi}}_k$ has the smallest variance. An unbiased estimator for the variance is

$$V_k = \frac{1}{4}\left[\left\| \mathbf{R}_2(S_k) - \mathbf{R}_1(S_k) \right\|^2 \right] \tag{1.7}$$

The quantity in equation 1.7 follows a gamma distribution with shape parameter 1 and scale parameter σ^2, making it an unbiased estimator for σ^2. By aggregating these estimates across a set of K stimuli $S_1, S_2, ..., S_K$ independently realized by the same process and presented under identical experimental conditions, it is possible to infer performance parameters without additional process assumptions. For example, the quantity in equation 1.8 is normally-distributed with mean σ^2 and variance $\frac{\sigma^4}{K}$. This estimator of σ^2 is commonly referred to as the double-pass noise estimate.

$$\hat{\sigma}^2 = \frac{1}{K}\sum_{k=1}^{K} V_k \tag{1.8}$$

Since the quantity in equation 1.6 is an unbiased estimator of $\boldsymbol{\phi}(S_k)$, the quantity in equation 1.9 is an unbiased estimator of $\boldsymbol{\beta}(S_k)$.

$$\hat{\boldsymbol{\beta}}_k = \hat{\boldsymbol{\phi}}_k - \mathbf{T}(S_k) \tag{1.9}$$

The quantity in equation 1.10 is an unbiased estimator of $\gamma(S_k)$.

$$\hat{\gamma}_k = \frac{1}{2}\Big[\left\|\mathbf{R}_1(S_k) - \mathbf{T}(S_k)\right\|^2 + \left\|\mathbf{R}_2(S_k) - \mathbf{T}(S_k)\right\|^2 \Big] \tag{1.10}$$

Chapter 2

Investigations into individual strategies for estimating central tendencies

2.1 Introduction

2.1.1 Why (estimators for) central tendencies matter

The concept of a central tendency is fundamental in statistics because statisticians often handle point estimates for quantitative inference. Central tendencies appear fundamental in how the visual system handles perceptual objects, and this is likely because they provide a compromise between representational simplicity and sufficiency for decisions related to object motion. In order to perform daily behaviors, the entire cognitive architecture needs information about multiple objects in the visual scene with complicated dynamics. To meet these demands, the visual system likely maintains a proverbial grab-bag of summary statis-

tics, and adaptively recruits members from the bag given the environment and goals of the organism. The key feature of these statistics is that they are latent properties of the stimulus that can be extracted almost automatically (i.e perceived without effort), and that they provide compact representations likely to be useful in a variety of tasks and environments.

2.1.1.1 Reasons to study human estimation strategies

Humans are remarkably accurate centroid estimators. An important finding that is evidenced in every chapter of this dissertation is that humans are systematically biased, and some aspects of the bias emerge from complex interactions of the stimulus and observer. In other words, some components of systematic bias are caused by the perceptual mechanisms of a typical human subject, but others are idiosyncrasies of a particular human. Classification of these bias components requires coupled experimental and theoretical work. Why should anyone bother? Two societal benefits are explained below.

Improved safety on highways shared by humans and autonomous machines

Point estimates of position and velocity are the most efficient representations of objects in a dynamic scene. While autonomous vehicles rely on these statistics to infer the consequences of motion, it is not currently understood how the same information is used by human drivers. There is some evidence to suggest humans have access to this information, and use it for decisions that are obviously relevant to impact probabilities. For example, humans use centroid estimates to judge relative positions (Hess et al., 1994; Badcock et al., 1996), direct gaze (He and Kowler, 1989; Kowler et al., 1995; Kowler and Blaser, 1995), and infer the stability of objects in 3-D (Cholewiak et al., 2015). However, it has also been shown that information about shape provides a sense of direction that coincides for multiple observers (Sigurdardottir et al., 2014). In particular, are there systematic estimation errors linked to

the mechanisms of neural coding or human perception? If so, self-driving cars could use this information to anticipate false alarms made by human drivers (by detecting conditions when those false alarms are more likely to occur). Unfortunately at this time, little information is freely available about these safety differences, mostly because an appropriate measure of performance has not been identified by experts. The investigation framework described here can provide insight on these problems.

Improved ergonomics

The distribution of mass determines the easiest way to lift a heavy object. How does a human infer the distribution of mass from visual cues available? In particular, which properties of shape or texture are misleading (i.e. most likely to cause estimation errors)? If so, understanding the mechanisms of perception for these tasks can be used to inform policy, and reduce the risk of workplace injuries.

2.1.2 Center representation in neural systems

Since Newton (1999), the center-of-mass has been recognized as an important predictor of motion in physical systems. The dynamics of a neural system can usually be described by the pursuit of equilibrium points (Izhikevich, 2007). In fact, modeled as a nonlinear system, the solutions for equilibrium points are equivalent to the solutions for balancing points of a physical system. When it comes to changes in stable points, the effect of varying light in the visual field is analogous to the effect of varying mass in the gravitational field. In other words, neural systems stabilize *given* the energies of their input. Changes in the state of the world drive changes in the stable points of the system, and the ability to re-equilibrate naturally is sufficient to account for some representations of centroid, but not all.

The cortical representation of visual objects is where the luminance-based centroid mechanism cannot account for experimental findings. Cortical representations of visual objects are contingent on perceptually salient boundaries, which are maintained as shaped-based features and contour fragments, independent of luminance information. Heightened sensitivity to contours has been demonstrated psychophysically (Hess et al., 1994), and explained with neural connections between spatially adjacent edge detectors with similar orientation tuning (Field et al., 1993). After this association, it appears perceptual boundaries are maintained independently of luminance information on the boundary. Regardless, there is evidence that shape-based features influence center perception or localization, even under conditions which emphasize the center-of-mass (Proffitt et al., 1983; Bingham and Muchisky, 1993a,b; Baud-Bovy and Soechting, 2001; Davi et al., 1992). Shape information has been shown to facilitate rapid visual search performance (Elder and Zucker, 1993), which suggests the mechanism is a modulation of tuning (David et al., 2008). Neural models of tuning to shapes assume a polar domain, which implies a central point around a population of neurons positioned at different angles and tuned to degrees of curvature (Pasupathy and Connor, 2002).

2.1.3 Center estimation in psychophysics

There is some evidence that humans use the center-of-mass to infer the stability of objects in 3-D environments (Cholewiak et al., 2015). There is substantial evidence that center-of-mass perception influences the way humans interact with physical objects, both by grasping (Bingham and Muchisky, 1993a,b; Crajé et al., 2013), and with gaze direction (He and Kowler, 1989; Kowler et al., 1995). Other kinds of centers, providing compact descriptions that are useful for guiding behavior or attention have been proposed from biology and demonstrated psychophysically (Kovács et al., 1998). Many investigations conclude that the visual system relies primarily on boundary information when performing tasks of perceptual alignment (Proffitt et al., 1983; Vos et al., 1993), or location discrimination (Hess et al., 1994). There

is certainly only a single point in space that is simultaneously closest to every point on the boundary. That point would provide the best spatial reference for boundary information. While this figural center might be spatially correlated with the center-of-mass, they are have distinct perceptual qualities.

The investigation of Proffitt et al. (1983) is one of the earliest psychophysical investigations into the idea that subjects use multiple sources of information in order to derive a centroid estimate. The two sources investigated were "configural" and "luminance-based." The stimuli were static or revolving shapes, with luminance distributions skewed (or not) by grading or stripes. The authors report that for both revolving and static stimuli, subjects' responses fall closer to the configural center than the luminance-based center. They also found that the luminance manipulation increases response variability, and this increase does not interact with shape symmetry. From this the authors speculate that luminance and configural information might be independent, or interact weakly. This study provides evidence that the location of perceived centers relies on boundary information.

Bingham and Muchisky (1993a,b) investigated the influence of shape, size, symmetry, and orientation of uniform bodies on center-of-mass perception. The investigators measured their subjects' estimates of the center-of-mass by grasping the objects with a pair of tongs. Their findings suggest the perceived point of equilibrium occupies a space spanned by the center-of-mass, but subjects rely primarily on boundary information to perform the task. These authors also report effects of symmetry on response variability, both random and systematic components. Specifically, they found variability tended to rise as symmetry declined. For the most asymmetric shapes, increasing size increased the random error. From this the authors speculate that increasing size might reduce the quality of boundary information.

Hess et al. (1994) provide evidence that features of the stimulus configuration change perceptual thresholds for center localization. The study links these to changes in information sources when judging the central tendency. Without feedback, subjects were asked to de-

termine whether the position of a cluster of Gabor elements fell to the right or left of an imaginary reference line. They found the strategy subjects used to localize the cluster depended on three factors: (1) The number of elements, (2) the radius of the cluster, and (3) shaped-based information related to symmetry. Notably, the perceptual thresholds under the strategies did not depend on orientation information.

Badcock et al. (1996) extended the results from Hess et al. (1994) in an attempt to identify the best-fitting center by adding a manipulation to vary the distribution of internal luminance. Using clusters with 1, 10, or 100 elements, psychometric thresholds for real observers were calculated and compared to thresholds for the center-of-mass, boundary midpoint, or peak of the luminance distribution. They found that the best-fitting center changed as a function of the number of elements. For stimuli with few elements, the central tendency coincided with the location of peak luminance. At intermediate numerosities, the central tendency fell closer to the boundary midpoint. As the number of elements approached 100, thresholds fell closer to the center-of-mass (although for these stimuli the center-of-mass tended to coincide with the boundary midpoint). Taken together, (Hess et al., 1994; Badcock et al., 1996) provide evidence that there is a mechanism sensitive multiple sources of center information, and that this mechanism can dynamically alter the contribution of each information source as a function of the stimulus configuration and task instructions.

Since subjects were not given feedback, the investigations by (Proffitt et al., 1983; Bingham and Muchisky, 1993a,b; Hess et al., 1994; Badcock et al., 1996) provide insight about which strategies humans find naturally compelling for center estimation.

2.2 Methods

2.2.1 Subjects

All methods were approved by the UC Irvine Institutional Review Board. 7 subjects (4 female) provided written consent to participate in the study. The ages ranged from 18 to 35. All subjects were students at the University of California, Irvine, with extensive experience in a variety of centroid tasks. The subjects consented to four sessions with sleep in between. All experimental sessions for a given task were completed within a week of the training session. Data from all four sessions are analyzed and reported in the results section.

2.2.2 Materials

All sessions were completed on a Dell desktop running the Windows 7 Professional operating system. Stimuli were generated in custom MATLAB code, and displayed using Psychophysics Toolbox (Brainard, 1997). Responses were collected on discretized pixel coordinates using an optical mouse connected to the desktop via wired USB. Subjects' viewing distance was fixed at 60 centimeters using a chin rest. From this distance, All stimuli were displayed inside a circular frame that was 28 degrees in diameter.

2.2.3 Procedure

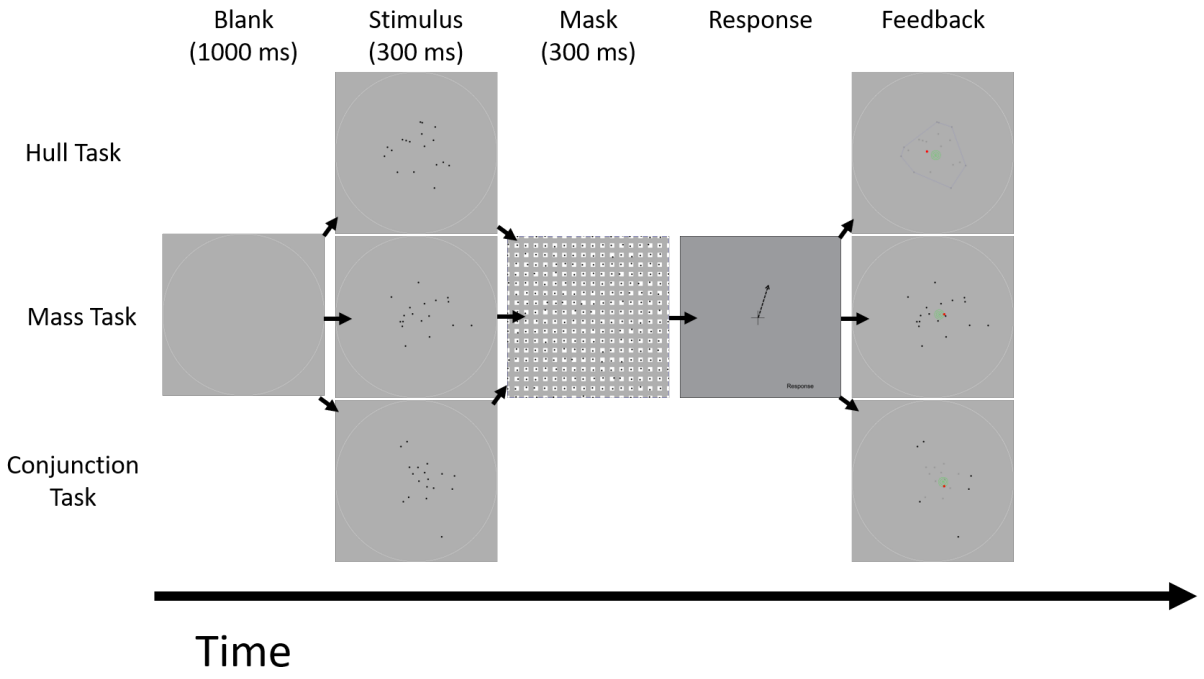

Figure 2.1: This figure illustrates the sequence of events in experimental trials of chapter 2. Events common to all three tasks are shown in the middle row. The top row shows a stimulus and feedback pair from the hull task. The middle row shows a stimulus and feedback pair from the mass task. The bottom row shows a stimulus and feedback pair from the conjunction task.

The sequence of events on each trial is illustrated in figure 2.1. After the subject initiated the trial, the events were as follows: The circular display for 1000 ms, followed by a dot cloud or singleton stimulus for 300 ms, followed by a post stimulus mask for 300 ms, followed by the blank display frame until recording the response, followed by the feedback. Finally a feedback display was presented including (a) the stimulus, (b) a green bullseye at the correct location, and (c) a red dot at the location of the subject's response. The subject was allowed to view this feedback for as long as desired before initiating the next trial.

Each subject completed three tasks over nine sessions (1 training and 2 experimental sessions per task). Each session consisted of twelve blocks of trials, with a chance to rest after each block. For a given subject, experimental sessions began around the same time of day as the training. To ensure consolidation of learned strategies during sleep, sessions were spaced at least a day apart. After being trained on a task, both experimental sessions were completed within a week, and subjects never performed more than one task per week.

2.2.4 Stimuli

600 stimuli per session were generated by the process described in Sun et al. (2013), and recapitulated here. Each stimulus comprised a random cloud of 18 black dots (disks with diameter subtending 0.2 deg.) presented on a mean gray (15.63 cd/m^2) background. Thus each dot had Weber contrast approximately equal to -1.

To generate a stimulus, we first obtain jointly independent standard normal random variables $\tilde{X}_1, \tilde{X}_2, \cdots, \tilde{X}_{18}$ and $\tilde{Y}_1, \tilde{Y}_2, \cdots, \tilde{Y}_{18}$.

Next, we derive

$$X_d = c\tilde{X}_d \quad \text{and} \quad Y_d = c\tilde{Y}_d$$

for c chosen to satisfy

$$\frac{1}{\sqrt{34}} \sum_{d=1}^{18} \left((X_d - \bar{X})^2 + (Y_d - \bar{Y})^2 \right) \quad = \quad 3 \text{ deg.}$$

where $\bar{X}$ ($\bar{Y}$) is the mean of the X_d's (Y_d's) for $d = 1, 2 \cdots, 18$, and the constant $\sqrt{34}$ is chosen to make the value 3 deg. equal to the unbiased estimate of the standard deviation of the circular, bivariate Gaussian distribution from which the locations (X_d, Y_d) were drawn. Next, the locations of the dots in the stimuli were (x_d, y_d), where

$$x_d \quad = \quad \mu_x + X_d \qquad \text{and} \qquad y_d \quad = \quad \mu_y + Y_d$$

for (μ_x, μ_y) a random point uniformly distributed around the circle centered in the middle of the display with radius 3.23 deg. Thus, the actual centroid of the locations (X_k, Y_k) was $(\mu_x + \bar{X}, \mu_y + \bar{Y})$.

Finally, if one or more dots escaped from the display boundary, or if the edge-to-edge separation between any pair of dots was less than a single pixel, the entire set was discarded and the process began again. Overall, the probability of discarding a stimulus for this reason remained less than 5 percent. Subjects were trained on a set of 600 stimuli generated by only this procedure. For the pair of experimental sessions, stimuli generated as above were further modified for the purposes of these experiments.

Modification 1: Increases expected distance between targets from different tasks

300 of the random dot clouds were modified to ensure the task-dependent target locations could be distinguished by distance. Specifically, the sampling process was constrained to accept a cloud only if it had three centers forming a triangle with an area greater than or equal to the area of an equilateral triangle with height of .5 degrees. These clouds are not Gaussian, but they provide a set of trials where subjects can unambiguously select one center over the others.

Modification 2: Strips some stimuli of internal mass

For experimental sessions, 25 percent of the stimuli in each set of 300 were randomly selected and stripped of internal dots to produce "Vertex-Only trials," (VO). These stimuli had fewer dots than the full set, but had the same expected area.

Modification 3: Singletons

10 percent of stimuli were randomly selected to become singleton trials. Singleton trial dots are positioned at the target center of the (unseen) stimulus cloud. By collecting singleton data, we can draw inferences about factors limiting performance in the absence of any estimation process.

To summarize, each experimental stimulus set transformed 600 random dot stimuli into 60 singleton stimuli, 150 vertex-only stimuli, and 390 full set stimuli. We generated two stimulus sets per subject, per task– one for a training session without modifications, and the other for two experimental sessions.

2.2.5 Task Conditions

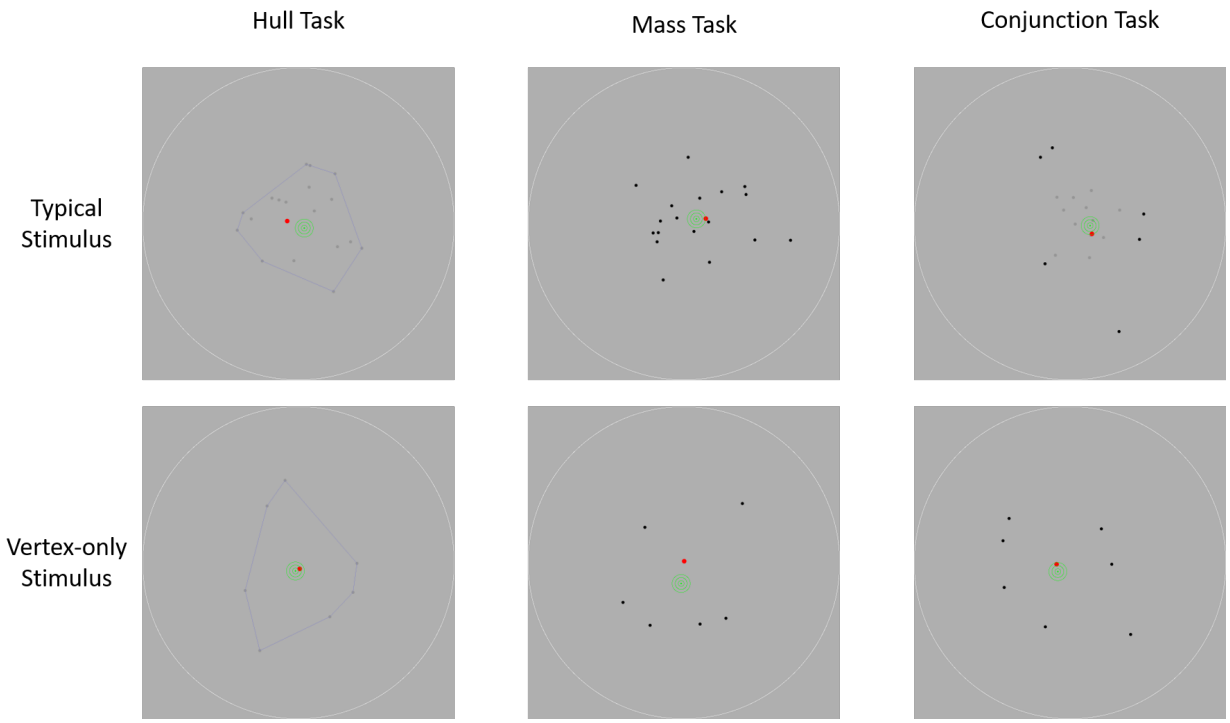

Figure 2.2: This figure shows feedback differences across all three tasks for the full stimuli (top panels) versus the vertex-only stimuli (bottom panels).

Every subject performed three variants of the centroid task with trial-by-trial feedback before and after training. In addition to showing the target and response locations, the feedback stimulus includes a version of the stimulus modified to accentuate the task-relevant part(s) (see figures 2.1 or 2.2). We now define each of these tasks in terms of their feedback and instructions.

Hull Task

A set of points is a convex set if one can can move in a straight line between any pair of points without leaving the set. In geometry, any convex polygon defines a convex set of points in 2D. Given a dot cloud stimulus, one can find the minimal convex set that covers all points in the stimulus. The mean position of all pixels in this convex set is the center of

the convex hull. We can also arrive at the hull center by connecting adjacent vertex pairs with straight edges, and then taking the mean of pixel positions that intersect the union of edges.

An example of the feedback displayed after each trial in the hull task is shown in the left side of figure 2.2. Feedback for the Hull Task was modified so dot contrasts were reduced to more closely match the background, and a straight-edge boundary was shown enclosing the minimal convex set covering the stimulus. Subjects were instructed to envision a rubber band snapping around the stimulus, and to indicate the center of the enclosed region.

Mass Task

In a uniform gravitational field, the center of mass for a set of points is the equilibrium point, (i.e. if the points are on the same surface, then it is the point on which the surface would balance). Given a set of dot positions, the center of mass is computed from a linear combination of the locations with uniform weighting function.

An example of the feedback displayed after each trial in the Mass Task is shown in the center of figure 2.2 . Because the ideal filter in the Mass Task is the uniform filter, we did not alter the contrast of dots in feedback stimuli. Subjects were instructed to treat each dot equally in terms of mass and to find the balancing point of the stimulus.

Conjunction Task

Perfect hull task performance would require the subject to apply a uniform weighting function to all pixels located on the convex hull, a uniform weighting function for all pixels located in the convex hull, or both. Perfect mass task performance would require the subject to apply a uniform weighting function to all pixels where dots are located (i.e. any pixel with same

luminance contrast as dots in the stimulus). Perfect conjunction task performance would require a uniform weighting function to all pixels located on the convex hull AND where dots are located. In other words, in the conjunction task, subjects are tasked with estimating the center of mass, but only for dots positioned on the convex hull (i.e. vertices).

An example of the feedback displayed after each trial in the conjunction task is shown in the right side of figure 2.2. By lowering the contrast of internal dots in feedback stimuli, subjects are instructed to treat each vertex equally in terms of mass and to find the balancing point, ignoring all other items.

2.3 Model

2.3.1 Preliminaries

Let $S_1, S_2, \cdots, S_K$ be a subset of the stimuli used in the double-pass procedure. Thus, for any stimulus in this set, for $\mathbf{R}_1(S_k) = (R_{1,x}(S_k), R_{1,y}(S_k))$ and $\mathbf{R}_2(S_k) = (R_{2,x}(S_k), R_{2,y}(S_k))$ are the responses to S_k on the first and second trials in which it is presented.

2.3.2 New quantities

The first newly defined quantity is an estimator for 1.5 over the set of K stimulus patterns presented under identical task conditions. By calculating the statistic 1.10 for every full stimulus S_k, $k = 1, 2, \cdots, K$ presented to a particular subject in a given task, we can estimate the parameter

$$\mathrm{E}[\gamma \mid \text{task}] \approx \frac{1}{K} \sum_{k=1}^{K} \hat{\gamma}_k$$

Figure 2.3 shows (the square root of) these estimates with standard error bars for comparison.

The second newly defined quantity is an estimator for 1.4 over the set of K stimulus patterns presented under identical task conditions. Since the quantity in equation 1.6 is an unbiased estimate of $\boldsymbol{\phi}(S_k)$, the quantity in 1.9 is an unbiased estimate of $\boldsymbol{\beta}(S_k)$. By calculating the statistic 1.9 for every full stimulus S_k, $k = 1, 2, \cdots, K$ presented to a particular subject in a given task, we can estimate the parameter

$$\mathrm{E}[\boldsymbol{\beta} \mid \text{task}] \approx \frac{1}{K} \sum_{k=1}^{K} \hat{\boldsymbol{\beta}}_k$$

Figure 2.4 shows these estimates with standard error bars for comparison.

The third newly defined quantity is the deletion effect parameter in task t. This parameter allows us to infer the effect of vertex-only stimuli on the precision of the subject's estimation strategy in task t. If σ_t^2 denotes the parameter from equation 1.2 when the stimulus pattern is as expected (i.e. not a vertex-only stimulus), and $\sigma_{t,\mathrm{vo}}^2$ is the parameter when the stimulus is not as expected, then the deletion effect is defined in equation 2.1.

$$\delta_t = \frac{\sigma_{t,\mathrm{vo}}^2}{\sigma_t^2} \tag{2.1}$$

This quantity takes values larger than 1 whenever the deletion of luminance cues inside the convex hull causes a loss of precision in the chosen estimation strategy (i.e. $\sigma_{t,\mathrm{vo}} > \sigma_t$). When it is less than 1, the presence of luminance cues inside the convex hull causes a loss of precision in the chosen estimation strategy (i.e. $\sigma_{t,\mathrm{vo}} < \sigma_t$).

The fourth newly defined quantity is an estimator for the deletion effect parameter. If $\hat{\sigma}_t^2$ is an estimate of the denominator in equation 2.1 obtained from the statistic in equation 1.8 applied to full stimuli presented to the subject in task t, and $\hat{\sigma}_{t,\mathrm{vo}}^2$ is the same applied

to vertex-only stimuli, then 2.2 is a performance statistic that makes predictions about the deletion effect testable.

$$\hat{\delta}_t = \frac{\hat{\sigma}^2_{t,\text{vo}}}{\hat{\sigma}^2_t} \tag{2.2}$$

Given our previous assumptions (equations 1.3 and 1.8), the quantity in equation 2.2 follows a scaled F distribution. The scaling coefficient is the deletion effect parameter, and the degrees of freedom are twice the number of stimulus patterns sampled to obtain the numerator and denominator. This property allows for statistical inference with a Bayesian or Frequentist framework. By bootstrapping equation 1.8 from the two types of stimuli in a given task, it is possible to sample from the distribution. Figure 2.6 shows estimates of the parameter E[δ | task] with standard error bars for comparison.

2.4 Results

2.4.1 Subjects are worst at the conjunction task

Figure 2.3 shows for all subjects $E[\hat{\gamma}|\text{task}]$ is substantially higher for the conjunction task than for either the mass or hull task. A reasonable question to ask is about the cause of this common trend–specifically, are all subjects worst at the conjunction task for the same reason? The results in figure 2.4 suggests the answer to this is no, at least if the common cause is an increase in systematic bias magnitude. Instead it appears that a more complicated model is required to explain how the common trend emerges from individuals using different strategies.

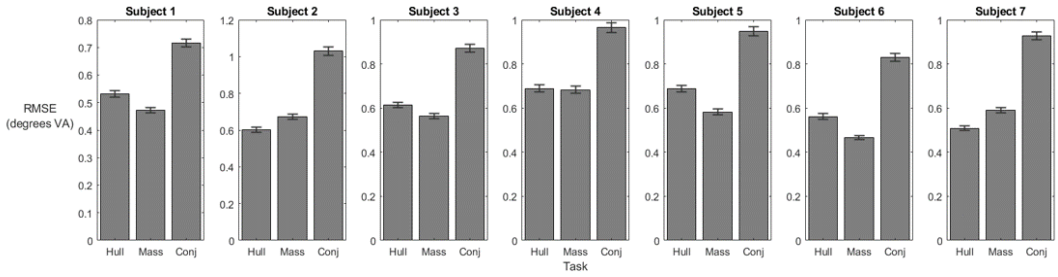

Figure 2.3: (square-root of) Estimates of the quantity defined with equation 1.10. $\sqrt{E[\hat{\gamma}|\text{task}]}$ on the vertical axis with standard error bars for comparison. Each panel shows results for a different subject in all three tasks responding to full stimuli only.

2.4.2 Systematic biases are small, but significant

Figure 2.4 shows how patterns of bias vary across subjects and tasks, (eq. 1.9 treating $x-$ and $y-$ components as independent and identically distributed univariates.) 5 out 7 subjects achieve a strategy successful enough to avoid detection of bias at the .05 level. Interestingly, this is true for two subjects performing the conjunction task (subjects 3 and 5). However, it appears that the chances of a given subject achieving this level of success in more than one task is low.

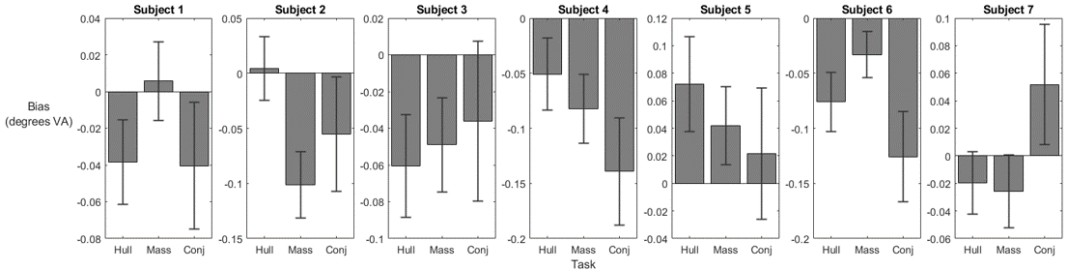

Figure 2.4: This figure shows patterns of estimation bias across subjects and tasks in chapter 1.

2.4.3 Most individual strategies are flexible

One way to show subjects are developing distinct strategies for each task is to calculate the Euclidean distance between responses and each of the three possible target locations in each

stimulus. If the subject is intentionally selecting the task-dependent target location, then we expect that target to be closer, on average, to the observed response location than either of its competitors. If subjects were not adapting estimation strategies in each task, then the results in figure 2.5 are extremely unlikely. Specifically, For subject s in task t, the panel in row t and column s of figure 2.5 shows the root-mean-square distance of the subject's responses in task t from the three possible target locations, labeled on the horizontal axis. For all subjects other than subject 5, responses in the mass and hull tasks tend to be closer to the correct target location. However, this is not true in the conjunction task, where responses tend to be farther from the target than the hull or mass center. This latter result suggests subjects are attempting to perform the conjunction task with some compromise between the strategies developed for the mass task and hull task.

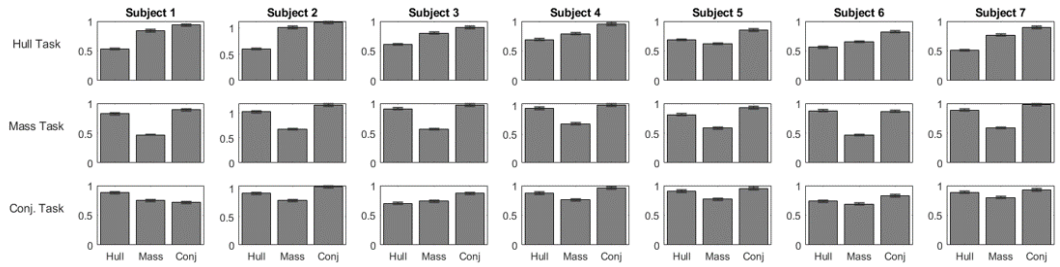

Figure 2.5: This figure shows evidence that subjects are able to control estimation strategies when given immediate visual feedback. For subject s in task t, the panel in row t and column s shows the root-mean-square distance of the subject's responses (to full stimuli only) in task t from what would be the target location in each of the hull, mass and conjunction tasks. The vertical axis is distance in degrees of visual angle. Standard error bars are shown for comparison. Note that (1) for all subjects, responses in the mass task are closer to the mass-task target location than they are to either of the hull- or conjunction-task target locations; (2) for 6 of 7 subjects, responses in the hull task are closer to the hull-task target location than they are to either of the mass- or conjunction-task target locations; however, (3) for 6 of 7 subjects, responses in the conjunction task are *farther* from the conjunction-task target location than they are from *either* the mass-task or the hull-task target location

2.4.4 The effect of vertex-only stimuli varies with subjects and tasks

Figure 2.6 shows how the precision of estimation strategies for each subject and task is affected by the unexpected deletion of cues typically available in the stimulus (eq 2.2). For all subjects performing the mass task, the estimated value of δ is greater than 1, which indicates a loss of precision on vertex-only trials. In the hull task, the effect varies across subjects, which indicates greater individual differences in the strategies chosen for this task. In the conjunction task, the estimated value of δ is less than 1 for 4 of 7 subjects, which indicates greater precision on vertex-only trials. For the remaining subjects, the estimated value of δ suggests precision is not affected by the difference.

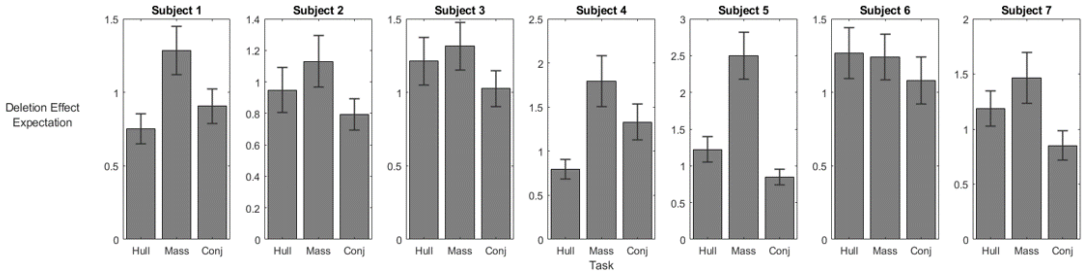

Figure 2.6: This figure shows estimates for the expected value of the deletion effect estimator, defined in equation 2.2, on the vertical axis with standard error bar for comparison.

2.5 Discussion

2.5.1 Most subjects develop a task-dependent strategy

The results illustrated in figures 2.5 and 2.6 together provide strong evidence that most subjects are able and willing to adjust their strategies for improved estimator performance, given immediate visual feedback. If the same estimation strategy was used on all three tasks, then the results illustrated in figure 2.5 should look similar to the results for subject

5. With the exception of subject 5, there is variation in estimates, which indicates changes in the estimator deployed by each subject. Furthermore, on vertex-only trials, the conjunction task and mass task produce identical feedback. If the same estimation strategy was used in the mass task and conjunction task, then then effects illustrated in figure 2.6 should be the same across these two tasks. There are factors of our design which may yield this result. For example, estimator performance for the mass task has been shown to asymptote at shorter timescales than the SOA used here. To our knowledge, the timescale for hull task performance asymptotes has no been measured empirically; however, based on computational models of neural processing (Pasupathy and Connor, 2002), it seems likely that more time is required for recurrent processing of available shape information to provide a stable percept of the convex hull. It is possible that mass and hull task performances might diverge when measured at shorter SOAs.

These findings are consistent with previous evidence that strategies vary with features of the task and stimulus configurations, and allow subjects to respond without feedback. For example, Proffitt et al. (1983), reported differences for subjects responding to static versus revolving stimuli. In conditions with a revolving stimulus, subjects reported their estimate of the center by positioning the stimulus so the shape appeared to spin without moving as a whole. In conditions with a static stimulus, subjects reported their estimate of the center by positioning the stimulus so the shape appeared centered on an arbitrary reference point. This change in the task created detectable differences between the subject groups in nearly every analysis reported. In the studies by (Hess et al., 1994; Badcock et al., 1996), strategies for localization were found to vary systematically with configurations of the cluster related to density and symmetry, but not with the orientation of individual elements. The models explain their results with a visual system that localizes things differently when the interior of a shape can be resolved.

Our results in the context of previous literature indicate that feedback is a necessary component of the centroid task, if the investigator wants the subject to attempt a particular strategy. Also, caution should be warranted for stimulus populations where the mass center and hull center are highly correlated, since this allows the subject to perform well on both tasks using the same strategy.

2.5.2 Implications for mechanisms of strategy and object-based vision

Our results are consistent with two distinct mechanisms for estimating central tendencies. The first uses variations in luminance across space in order to derive an estimator that is most like the center of mass. The second emerges from cortical representations of shape (i.e closed boundary, or contour fragments). Most subjects appear able to select the cue(s) available in one mechanism or the other, in order to perform the hull and mass task with comparable accuracy and precision. In contrast, conjunction task performance suggests there is not a third mechanism acting like a coincidence detector for the mechanisms used in both mass and hull tasks. In these experiments, all cues for the target location were variations in luminance intensity across space (i.e. dots), and whatever boundary the visual system is able to construct from the dot pattern. The deletion effects in figure 2.6 show the effectiveness of luminance-based cues *inside* the dot cloud varies systematically across tasks. This suggests that variations in luminance over space are qualitatively distinct when the space belongs to a visual object. This is consistent with previous research that suggests contour perception does not depend on luminance information available at the boundary of an object. For example, Proffitt et al. (1983) report no effect of luminance on the boundary of figures. In a very different experimental paradigm, Field et al. (1993) report the perception of continuity is stable, even when gaps in the contour are much larger than the individual items, or when adjacent elements were oriented up to +/- 60 degrees relative to each other.

Furthermore, Hess et al. (1994), used clusters of Gabors of variable orientation to estimate perceptual thresholds across orientation-selective channels, and report localization thresholds are invariant to clusters of mixed orientations. This suggests the mechanism of localization is insensitive to the orientation information available in luminance-based response of simple edge detectors. Taken together, these studies suggest that a perceptual centers based on contours does not depend on response of simple edge detectors.

Since Attneave (1954), it has been widely accepted that shape plays an important role in object recognition. Many authors have conjectured on the cause of this relationship. The information theoretic account claims sharp boundaries are less likely to occur by chance, so attending to contours is one way to maximize the information sampled from a visual scene. Psychophysical evidence is consistent with this view, and has been used to argue shape information can help guide rapid visual search (Elder and Zucker, 1993). In other behavioral paradigms, shape has been shown to provide a sense of direction that coincides for multiple observers (Sigurdardottir et al., 2014). Based on the literature extending from Attneave (1954), one might expect points with the greatest curvature to be the most salient. Some authors have taken this idea further, claiming the visual system partitions the visual field into the least overall negative curvature (i.e. as many convex shapes as possible) because this is the simplest configuration (Feldman and Singh, 2005).

Cortical representations of shape vary across regions of the visual cortex (David et al., 2006; Craft et al., 2007), and beyond (Sereno and Maunsell, 1998). It has been argued that the representational variability is explained by functional differences across regions of the cortex (Lehky and Sereno, 2007). In V1, edge information is represented as localized and orientation-dependent variations in luminance contrast (i.e. Gabor-like receptive fields). In V2, cells with similar orientation tuning are linked over longer distances to form illusory contours, independently of complete edge information (Hess et al., 2003; Von der Heydt et al., 1984). Empirical evidence and modeling suggest border ownership signals in V2 or V4

can be integrated by later cortical processing to form representations of a shape's interior (Tschechne and Neumann, 2014). For example, border-ownership signals have been shown to modulate neural responses differently when attention is manipulated (Qiu et al., 2007). The cortical response to stimuli falling outside the classical receptive field can be modulated by lateral connections within the same level, and feedback connections from higher levels. These models are supported by psychophysical experiments with small primates (Roelfsema et al., 1998, 2002), where the psychophysical object-based processing advantages have been reported. According to (Konen and Kastner, 2008), the neocortex uses shape and other features to maintain a hierarchically-distributed representation of visual objects. These distributed representations can account for object-processing advantage measured in primate behavioral experiments(Roelfsema et al., 1998, 2002).

2.5.3 There is evidence for systematic biases in most estimation strategies

Previous investigations into center estimation aggregate data across subjects. Figure 2.7 shows why the systematic biases reported in figure 2.4 become harder to detect in all three tasks when data are treated this way– the direction of bias from different subjects tends to cancel out. If one assumed a single noise term and pooled data across subjects, the simplest explanation for impaired conjunction task performance is an increase in variance. Obviously this is misleading, and fails to recognize the structure that emerges when looking at individual differences.

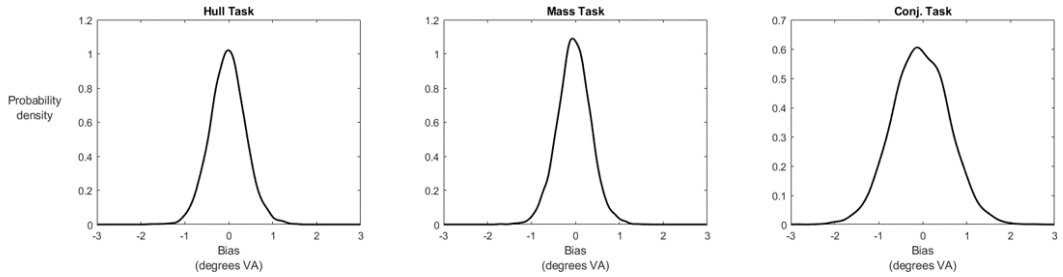

Figure 2.7: This figure shows patterns of estimation bias across tasks for chapter 1. Each panel shows a density kernel estimated from the bias components from figure 2.4 pooled across subjects. Note that all three distributions appear roughly symmetric and centered on 0, and the conjunction task appears to have a greater variance.

Chapter 3

Investigations into a neurophysiological account of estimation bias

3.1 Introduction

3.1.1 A parametric approach to explaining systematic bias

Chapter 2 shows evidence of systematic biases in the center-of-mass judgements made by our subjects. We would like to motivate the investigation of chapter 3 with a reparameterization of bias from equation 1.4.

If we impose the following assumption on the functional form of $\boldsymbol{\phi}(S)$ from equation 1.1:

$$\boldsymbol{\phi}(S) = \sum_{d=1}^{N} \omega_d(S) \begin{bmatrix} x_d \\ y_d \end{bmatrix}$$

where the N-dimensional vector of coefficients $\boldsymbol{\omega}(S)$ is constrained to sum to 1 (i.e. $\boldsymbol{\omega}(S)$ is a convex linear combination of all N dots in the stimulus S), then the estimation bias parameter $\boldsymbol{\beta}(S)$ can be expressed as in equation 3.1.

$$\boldsymbol{\phi}(S) - \mathbf{T}(S) = \sum_{d=1}^{N} \left(\omega_d(S) - \frac{1}{N} \right) \begin{bmatrix} x_d \\ y_d \end{bmatrix} \tag{3.1}$$

This reparameterization suggests it is possible to explain the source(s) of systematic error in terms of deviations from the uniform weighting function. If a parametric model of $\boldsymbol{\omega}(S)$ used features found in any stimulus to predict the bias, then it is possible to measure the influence of these features on the subject's strategy.

In chapter 3, we illustrate the usefulness of this approach by providing insight on a neurophysiological explanation for systematic biases called the density effect. Since theories of computation in neuroscience rely on behavioral data collected under conditions that preclude the use of human subjects, psychophysical paradigms where neurocomputational theories can be tested with human subjects is important now, perhaps more than ever. Chapter 3 additionally illustrates how the centroid paradigm provides an non-invasive and inexpensive candidate for these kinds of investigations.

3.1.2 A neurophysiological explanation for the density effect

The density effect is a tendency for subjects to underweight dots in densely populated regions of the stimulus relative to dots in sparsely populated regions (Moreland and Boynton, 2017; McGowan et al., 1998). To account for this density effect, Moreland and Boynton (2017) proposed that the subject's response is derived by computing the centroid of a nonlinear transformation of the stimulus. We can think of this transformation as being accomplished by

a retinotopically organized array of neurons (e.g., in primary visual cortex) whose collective response to the stimulus can be viewed as a "neural image" (Robson, 1980). It is assumed that the response of each neuron in this array is an increasing but compressive function of the number of dots that fall within its receptive field. (I.e., for $N > 1$, the activation of a neuron whose receptive field subsumes N dots is lower than the summed activations of N neurons each of whose receptive fields subsumes a single dot). Because of this compressive nonlinearity, a dot from a densely populated region of the stimulus will produce lower total net activation in the neural array than a dot from a sparsely populated region. Thus, the centroid of the neural image produced by the stimulus will be influenced less effectively by dots from densely vs. sparsely populated regions.

Although this model accounts neatly for the results of Moreland and Boynton (2017), it raises some important questions outside the scope of their study. First, are the neurons in the hypothesized array sensitive to contrast-polarity: i.e., do black vs. white dots influence these neurons with opposite sign? Substantial evidence suggests that the answer to this question is no: if the neurons mediating performance in centroid-estimation tasks were influenced with opposite sign by black vs. white dots, then it would be difficult to ignore contrast polarity in estimating the centroids of displays comprising mixtures of black and white dots. However, subjects perform this task with ease (Drew et al., 2010).

A subtler issue is the following: From the study of Moreland and Boynton (2017) we know that two dots of the same polarity that occur in close proximity interact to reduce the influence they jointly exert on the subject's centroid estimate. Is this also true if the dots have opposite contrast polarity? The following scenario suggests that the answer to this question might be no:

Consider a centroid-estimation task that uses stimuli composed of half white (positive contrast polarity) and half black (negative polarity) dots on a gray background. Suppose that:

1. The neural image from which the subject extracts the centroid is obtained by adding together the responses of on-center and off-center neural arrays. Under this scenario, the site of the compressive nonlinearity is a complex cell, and the density effect will persist regardless of differences in polarity.

2. The activation of a given on-center neuron is a compressive function of the number of bright dots that fall in its receptive field (but invariant with respect to the number of dark dots), and similarly the activation of a given off-center neuron is a compressive function of the number of dark dots that fall in its receptive field (but invariant with respect to the number of bright dots). In either of these scenarios, the site of the compressive nonlinearity is a simple cell, and the density effect will not persist when adjacent dots have opposite polarities.

Experiment 1 was designed to investigate this issue.

3.2 Experiment 1

3.2.1 Methods

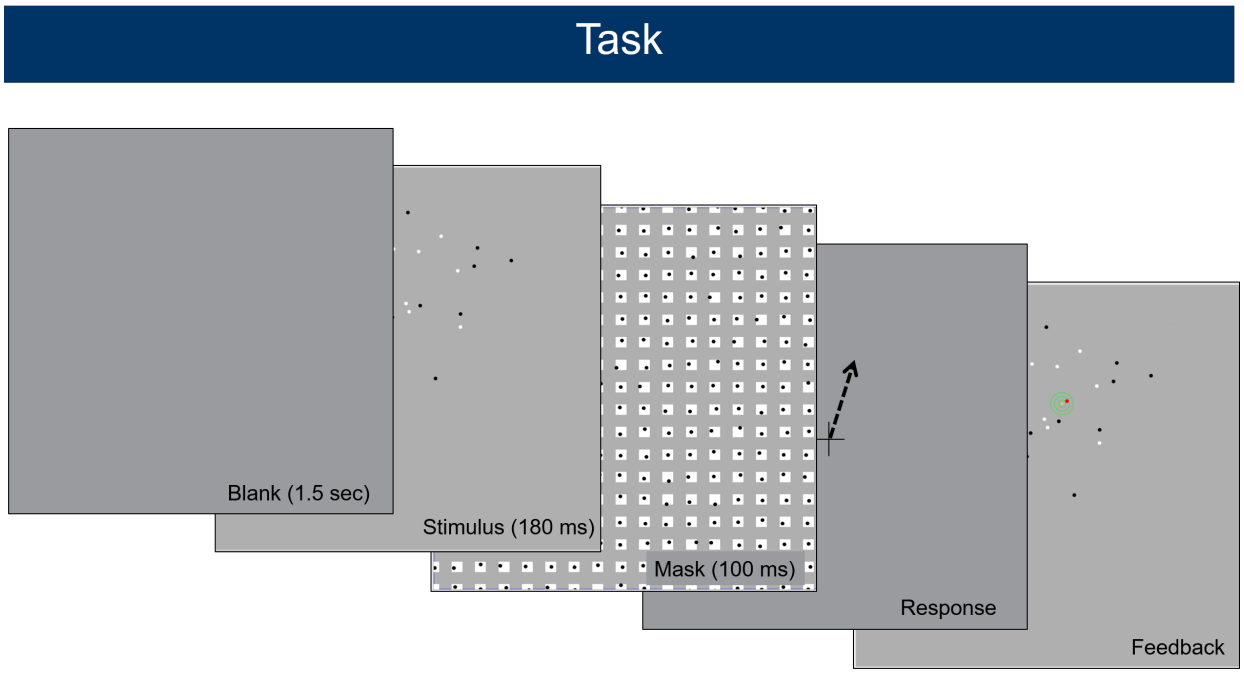

Figure 3.1: This figure illustrates the sequence of events in experimental trials of chapter 3.

3.2.1.1 Subjects

All methods were approved by the UC Irvine Institutional Review Board. 7 subjects (4 female) provided written consent to participate in the study. The ages ranged from 20 to 30. All subjects were students at the University of California, Irvine, with extensive experience in a variety of centroid tasks. The subjects consented to four sessions with sleep in between. Data from all four sessions are analyzed and reported in the results section.

3.2.1.2 Stimuli

A stimulus comprised a random cloud of 9 black dots and 9 white dots (disks with diameter subtending 0.2 deg.) presented on a mean gray (15.63 cd/m^2) background. Thus black and white dots had Weber contrasts approximately equal to -1 and 1. To generate a stimulus, we first obtain jointly independent standard normal random variables $\tilde{X}_1, \tilde{X}_2, \cdots, \tilde{X}_{18}$ and

$\tilde{Y}_1, \tilde{Y}_2, \cdots, \tilde{Y}_{18}$. Next, we derive

$$X_k = \gamma \tilde{X}_k \quad \text{and} \quad Y_k = \gamma \tilde{Y}_k$$

for γ chosen to satisfy

$$\frac{1}{\sqrt{34}} \sum_{k=1}^{18} \left((X_k - \bar{X})^2 + (Y_k - \bar{Y})^2 \right) \quad = \quad 3 \text{ deg.}$$

where $\bar{X}$ ($\bar{Y}$) is the mean of the X_k's (Y_k's) for $k = 1, 2 \cdots, 18$, and the constant $\sqrt{34}$ is chosen to make the value 3 deg. equal to the unbiased estimate of the standard deviation of the circular, bivariate Gaussian distribution from which the locations (X_k, Y_k) were drawn. Finally, the locations of the dots in the stimuli were (x_k, y_k), where

$$x_k \quad = \quad \mu_x + X_k \qquad \text{and} \qquad y_k \quad = \quad \mu_y + Y_k$$

for (μ_x, μ_y) a random point uniformly distributed around the circle centered in the middle of the display with radius 3.23 deg. Thus, the actual centroid of the locations (X_k, Y_k) was $(\mu_x + \bar{X}, \mu_y + \bar{Y})$.

If one or more dots escaped from the display boundary, or if the edge-to-edge separation between any pair of dots was less than a single pixel, the entire set was discarded and the process began again. Overall, the probability of discarding a stimulus remained less than 5 percent. After the positions were accepted, 9 of the 18 dots were randomly assigned membership to the set of black dots; the other 9 were assigned membership to the set of white dots.

3.2.1.3 Procedure

Subjects' viewing distance was fixed at 60 centimeters using a chin rest. From this distance, all task-relevant events were displayed using Psychophysics Toolbox (Brainard, 1997). On each trial, the stimulus cloud was surrounded by a thin, square black frame (width = 28 degrees of visual angle).

The set of events on each trial are illustrated in Fig. 3.1. The participant initiated each trial with a buttonpress. Then (1) a blank field was presented for 1500ms, (2) the stimulus cloud was presented for 150ms, (3) a blank field was presented for 30ms, and (4) a post-stimulus mask was presented for 100ms. Then the subject used a mouse to move a cross-hair cursor that appeared in the middle of a blank screen to mouse-click the location she judged to be the centroid of the stimulus cloud. Finally a feedback display was presented including (a) the stimulus, (b) a green bullseye at the correct location, and (c) a red dot at the location of the subject's response. The subject was allowed to view this feedback for as long as desired before initiating the next trial.

Each subject participated in four sessions. Each session contained 10 blocks. Each block contained 45 trials.

In order to obtain a model-free estimate of the noise compromising performance, this experiment employed a "double-pass" procedure. For a given subject, 900 stimuli, $S_1, S_2, \cdots, S_{900}$, were generated prior to testing. Across the 450 trials of session 1, the subject was presented with stimuli $S_1, S_2, \cdots, S_{450}$. In session 2, the subject was presented with $S_{451}, S_{452}, \cdots, S_{900}$. In Session 3 (Session 4), the subject experienced exactly the same set of 10, 45-stimulus blocks that had been presented in Session 1 (Session 2) preserving the order of stimuli in each block; however, the order of the 10 blocks was randomly shuffled.

3.2.2 Model

We use the logic of equation 3.1 to formulate a parametric model for $\boldsymbol{\phi}(S)$ which can be used to investigate for bias caused by non-uniformity in the weights.

3.2.2.1 Preliminaries

We write S_k for the $k-$th stimulus pattern presented to any particular subject. We write $(x_{d,k}, y_{d,k})$ for the $x-$ and $y-$ coordinates of dot d in this stimulus.

We write θ for the vector of parameters that can be varied in order to maximize the likelihood of observed responses.

We write $w_{d,k}$ for the weight dot d exerts on the subject's estimated target location when presented with S_k. These weights are a function of the stimulus and parameters, but we leave the parameter argument suppressed for simplicity.

We write $\boldsymbol{\varphi}(S_k;\theta)$ for the parametric model applied to stimulus S_k given parameters θ.

3.2.2.2 New quantities

The parametric estimator for chapter 3 is defined in equation 3.2.

$$\boldsymbol{\varphi}(S_k;\theta) = \begin{bmatrix} \beta_x \\ \beta_y \end{bmatrix} + \sum_{d=1}^{18} w_{d,k} \begin{bmatrix} x_{d,k} \\ y_{d,k} \end{bmatrix} \tag{3.2}$$

We start by describing how this model captures sources of estimation bias. Then we describe the nesting configurations.

3.2.2.3 Additive Biases

The first two components of θ are the parameters (β_x, β_y). This pair of parameters capture components of bias that do not vary with incidental features of the stimulus items. They provide the simplest possible description of a biased centroid estimator.

3.2.2.4 Feature Statistics

The main question of interest is: What features of the stimulus can account for the subjects estimation bias over many different stimuli? The analysis described in this chapter focuses on the Weber contrast (3.5), peripherality (3.6), and density (3.7). Of particular interest is the component of density orthogonal to peripherality (i.e. residual density from equation 3.9). Below we will formally define feature statistics c, p, and Δ that together capture the effects we intend to study. First we show how our parametric model can be used to explore the idea proposed in equation 3.1 with a regression-like model of the weighting function.

We assume impact exerted by a given dot d in stimulus S_k is a function of three model parameters (α_c, α_p, and α_Δ). We define this function in equation 3.3.

$$f_{d,k} = 1 + \alpha_c \; c_{d,k} + \alpha_p \; p_{d,k} + \alpha_\Delta \Delta_{d,k} \tag{3.3}$$

Note that if $\alpha_c = \alpha_p = \alpha_\Delta = 0$, then all dots receive equal weight, and the model $\boldsymbol{\varphi}(S)$ will only capture biases in terms of additive constants (β_x, β_y). Otherwise, dot weights deviate from equality with relative strengths that depend on α_c, α_p, and α_Δ. Therefore these parameters describe the source(s) of systematic bias using a regression-like model of dot weights.

Equation 3.4 imposes the unity constraint, relating equations 3.2 and 3.3.

$$w_{d,k} = \frac{f_{d,k}}{\sum_{j=1}^{18} f_{j,k}} \tag{3.4}$$

Contrast Polarity

We write $c_{d,k}$ for the Weber contrast of dot d in stimulus S_k

$$c_{d,k} = \begin{cases} -1 & \text{if dot } d \text{ is black in } S_k \\ +1 & \text{if dot } d \text{ is white in } S_k \end{cases} \tag{3.5}$$

Peripherality

We quantify the peripherality of dot d as follows. For any dot d, let $Q_k(d)$ be the Euclidean distance of d from the centroid of S_k (i.e. the stimulus in which it occurs). Then let $\pi_{d,k}$ be the proportion of dots from the entire set of stimuli presented to the subject which are closer to the centroid of the stimulus in which they occur than $Q_k(d)$.

$$p_{d,k} = \Phi^{-1}(\pi_{d,k}) \tag{3.6}$$

Where Φ^{-1} is the inverse normal cumulative distribution function.

Subjective Density

In order to define $\Delta_{d,k}$, we first need to define $z_{d,k}$, the density of the context surrounding dot d in stimulus S_k. $z_{d,k}$ captures information about the pairwise distances of all other dots e from dot d and also in stimulus S_k. It has three (subject-dependent) parameters that

describe how this information is aggregated over spatial scales within and across polarity channels.

Suppressing with stimulus index variable k, we quantify the density of the context of a dot d as follows:

$$z_d = \sum_{\substack{\text{dots } e \neq d \\ \text{with} \\ c_d = c_e}} f_{\text{same}}\left(\|v_e - v_d\|\right) \quad + \quad \sum_{\substack{\text{dots } e \\ \text{with} \\ c_d \neq c_e}} f_{\text{oppo}}\left(\|v_e - v_d\|\right) \tag{3.7}$$

where

$$f_{\text{same}}(q) = \cos^2\left[\frac{\pi}{4} + \rho\right] \exp\left[\frac{-q^2}{2\tau_{\text{same}}^2}\right] \quad \text{and} \quad f_{\text{oppo}}(q) = \sin^2\left[\frac{\pi}{4} + \rho\right] \exp\left[\frac{-q^2}{2\tau_{\text{oppo}}^2}\right]. \tag{3.8}$$

The parameter ρ controls the relative strength with which dots e of the same vs. opposite polarity as d influence the density of d's context. The parameter τ_{same} controls the the distance across which dots e of the same polarity as d influence the density of d's context, and τ_{oppo} controls the the distance across which dots e of opposite polarity influence the density of d's context.

Residual Density

Since our clouds are approximately Gaussian, any measure of density will be negatively correlated with peripherality observed over the course of the experiment. To decorrelate density relative to peripherality, we focus on the component of $z_{d,k}$ orthogonal to $p_{d,k}$. This is given by

$$\Delta_{d,k} = z_{d,k} - \left(\hat{b}_0 + \hat{b}_1\ p_{d,k}\right) \tag{3.9}$$

where $\hat{b}_0$ and $\hat{b}_1$ are obtained via linear regression so as to minimize $\sum \Delta_{d,k}^2$, where the sum is over all dots d presented over the course of the experiment. After this decorrelation, the residuals were rescaled to have unit variance.

What is reflected by the residual density characterizing the context of a given dot d? Because our stimulus clouds are distributed as bivariate normals, the contexts characterizing dots that are farther-than-average from the centroid of the stimulus cloud (i.e., dots $p_{d,k} > 0$) tend to have lower-than-average density. This is the root of the strong negative correlation between $z_{d,k}$ and $p_{d,k}$. The residual density $\Delta_{d,k}$ characterizing the context of d reflects the deviation of $z_{d,k}$ from the average density of dots with the same peripherality as d. In essence, then, $\Delta_{d,k}$ reflects the deviation of $z_{d,k}$ from what we might expect, given $p_{d,k}$.

3.2.2.5 Nested Configurations

Parameter	**unbiased**	**fixed bias**	**DPB bias**	**Full model**
β_x	0	free	free	free
β_y	0	free	free	free
α_c	0	0	free	free
α_p	0	0	free	free
α_Δ	0	0	free	free
ρ	-	-	0	free
τ_1	-	-	free	free
τ_2	-	-	τ_1	free
σ	free	free	free	free
P	0	2	6	8

Table 3.1: This table shows the nesting configurations for the model-based inferences regarding the sources of estimation bias. Cells marked "free" indicate which parameters are allowed to vary (see table 3.2 for the prior densities on each parameter). Cells containing numerical values indicate fixed parameters. Cells containing a - indicate parameters made void by a fixed parameter.

Equation 3.10 shows an equivalent expression for equation 3.2 when restricted to the no bias model (i.e θ_0).

$$\boldsymbol{\varphi}(S;\theta_0) = \mathbf{T}(S) \tag{3.10}$$

Equation 3.11 shows an equivalent expression for equation 3.2 when restricted to the fixed bias model (i.e. θ_2).

$$\boldsymbol{\varphi}(S;\theta_2) = \begin{bmatrix} \beta_x \\ \beta_y \end{bmatrix} + \mathbf{T}(S) \tag{3.11}$$

The remaining configurations (θ_6 and θ_8) allow for systemic bias components to vary with the 3 feature statistics evaluated for every item in the stimulus. We refer to the model restricted to θ_6 as the density-is-polarity-blind model (i.e. DPB model). The DPB model is identical to the full model with the constraint that $\rho = 0$ and $\tau_{\text{same}} = \tau_{\text{oppo}}$. By comparing the fit provided by the DPB model to that provided by the full model, we can assess whether dots of polarity opposite to that of a given dot d operate differently from dots of the same polarity to influence the density of d's context.

3.2.3 Results

Main Effects of Color, Peripherality, and Residual Density

The estimates of α_c, α_p and α_Δ four all seven subjects are plotted in figures 3.2, 3.3, and 3.4.

Black dots exert slightly more weight than white dots.

As shown in figure 3.2, the expected value of α_c is negative given data for all of our subjects. However, the 95% credible intervals contain 0 for four out of seven subjects. The strongest effect is shown by Subject 5, who has $\alpha_C = -0.066$, implying that for this subject black dots exert (on average) 14.2% more weight than white dots.

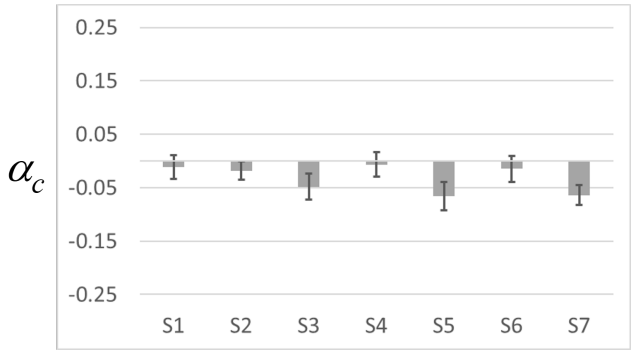

Figure 3.2: This figure illustrates posterior expectations and 95% credible intervals of the parameter α_c, for all subjects who participated in experiment 1.

Peripherality exerts significant influence whose direction varies across subjects.

As shown in figure 3.3, the effect of dot peripherality is statistically significant for 6 of 7 subjects although the direction of the effect varies across subjects. Individual differences akin to the ones observed here were also noted by Drew et al. (2010).

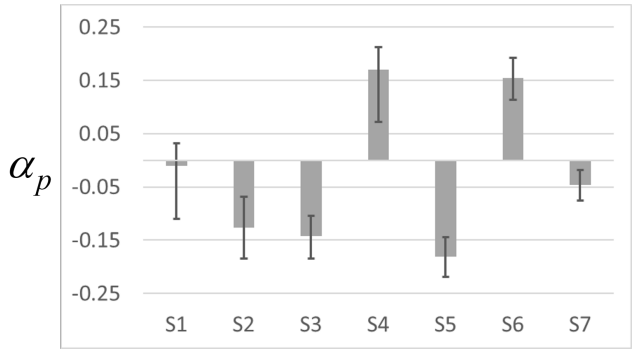

Figure 3.3: This figure illustrates posterior expectations and 95% credible intervals of the parameter α_p, for all subjects who participated in experiment 1.

To get a sense of the magnitude of this effect, consider the case of subject 5, who showed the strongest effect of peripherality with $\alpha_p = -0.181$. Dot peripheralities ranged from roughly -3.67 to 3.67, with dots very near the centroid of the stimulus in which they occurred receiving large negative values and dots very far from the centroid receiving large positive values. However, by construction, the distribution of $p_{d,k}$ values was (standard) normal; thus 95% of all dots d had $-1.96 < p_{d,k} < 1.96$. For subject 5, a dot with peripherality -1.96 (1.96) would (on average) exert 35% more (less) weight than a dot with periperality 0 (i.e., a dot of average distance from the center of the cloud).

Residual density exerts strong negative influence on dot weight for all subjects.

As shown in figure 3.4, α_Δ is significantly negative for all subjects indicating that dots occurring in contexts whose density is lower than average given their peripherality exert more weight than dots occurring in contexts whose density is higher than average given their peripherality. Since $\Delta_{d,k}$ was decorrelated with $p_{d,k}$, the effects associated with these two parameters on equation 3.3 are statistically independent.

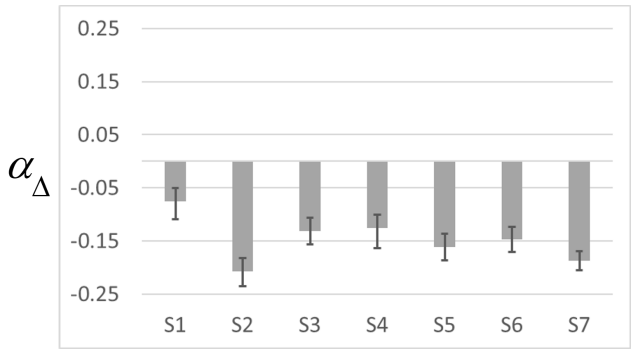

Figure 3.4: This figure illustrates posterior expectations and 95% credible intervals of the parameter α_Δ, for all subjects who participated in experiment 1.

To get a sense of the magnitude of this effect, consider subject 2. The values of $\Delta_{d,k}$ across all dots d and stimuli S_k conform approximately to a standard normal distribution. Subject 2 has $\alpha_\Delta \approx -0.2$. For subject 2, then, a dot with residual density -1.96 (1.96) would (on average) exert 39% more (less) weight than a dot with residual density 0 (i.e., a dot whose local context is of average density given its peripherality).

Spatial additive biases.

As shown in figure 3.5, for four subjects either or both of β_x and β_y differed significantly from 0. In all cases, however, they were also quite small– For all subjects each of these parameters was less that 0.17° of visual angle. Curiously, for all 7 subjects, β_y is negative.

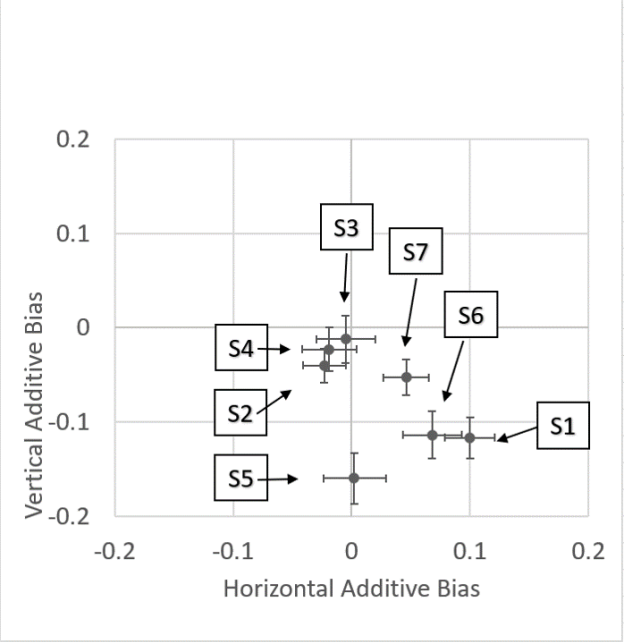

Figure 3.5: The parameters (β_x, β_y) for all subjects who participated in experiment 1. Points show posterior expectations. Error bars show 95% Bayesian credible intervals.

The parameters β_x and β_y capture constant additive biases in the subject's responses in order to account for components of estimation bias that cannot be explained by variability in the feature statistics investigated here.

The density of a dot's context.

A central question motivating this study was whether or not the density of the context of a given dot d was influenced similarly or differently by dots of the same vs. opposite polarity to d. The answer to this question is to be seen by considering the parameters $\rho, \tau_{\text{same}}, \tau_{\text{oppo}}$.

The parameter ρ determines the relative influence exerted on $z_{d,k}$ by dots of the same vs. opposite polarity to d and also in stimulus S_k. If $-\frac{\pi}{4} < \rho < 0$, dots of the same polarity as d will exert greater influence on $z_{d,k}$ than dots of the opposite polarity. If $0 < \rho < \frac{\pi}{4}$, the opposite is true. If $\rho = 0$, then dots of both the same and opposite polarity will exert

equal influence on the $z_{d,k}$. As shown in figure 3.6, the credible intervals for ρ for all subjects include 0, failing to reject the null hypothesis that dots of the same vs. opposite polarity of a given dot d exert different influence on $z_{d,k}$.

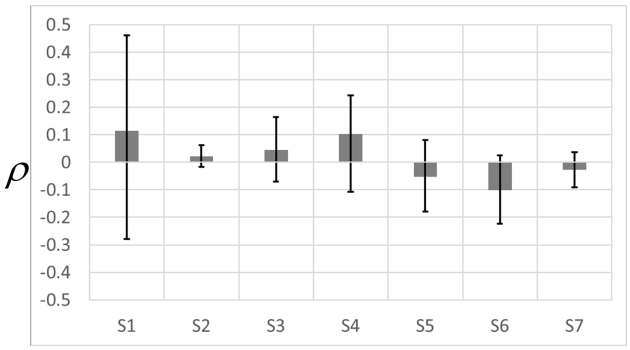

Figure 3.6: The parameter ρ for all subjects who participated in experiment 1. Height of the bar shows posterior expectation. Error bars show 95% Bayesian credible intervals.

The parameter τ_{same} (τ_{oppo}) determines the distance across which dots of the same (opposite) polarity as a dot d can influence z_d. For example, if τ_{same} is small, this indicates that dots of the same polarity as d will influence z_d only if they are close to d. If τ_{same} differs significantly from τ_{oppo}, this implies that dots of the same vs. opposite polarity as a dot d influence z_d across different spatial scales. As is evident from figure 3.7, for each subject the credible intervals for τ_{same} and τ_{oppo} overlap substantially suggesting that these parameters do not differ significantly.

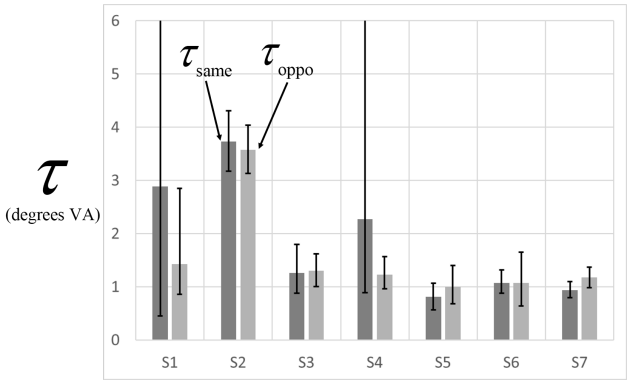

Figure 3.7: The parameters τ_{same} and τ_{oppo} for all subjects who participated in experiment 1. Height of the bar shows posterior expectation. Error bars show 95% Bayesian credible intervals.

Model Selection

Parameter	density	lower bound	upper bound	mean	variance
β_x	normal	-	-	0	A^2
β_y	normal	-	-	0	A^2
α_c	uniform	-1	+1	-	-
α_p	uniform	-1	+1	-	-
α_Δ	uniform	-1	+1	-	-
ρ	uniform	$-\pi/4$	$+\pi/4$	-	-
τ_1	exponential	-	-	3 degrees	-
τ_2	exponential	-	-	3 degrees	-
σ	uniform	0	A	-	-

Table 3.2: This table shows the prior densities used to calculate the Savage-dickey density ratios for model selection in both experiments for chapter 3. The constant denoted A is the width of the experimental display (28 degrees of visual angle).

The results for the parameters ρ, τ_{same} and τ_{oppo} suggest that the DPB model (in which the computation of $z_{d,k}$ is blind to the polarities of all dots in the display) may fit the data as well as the full model. This is supported by the Savage-Dickey density ratios (Wagenmakers et al. (2010)) for experiment 1, reported in table 3.3.

	$\beta_x = 0$	$\beta_y = 0$	$\alpha_c = 0$	$\alpha_p = 0$	$\alpha_\Delta = 0$	$\rho = 0$	$\tau_{\text{same}} - \tau_{\text{oppo}} = 0$
S1	>1000	>1000	0.023	0.164	>1000	1.378	2.827
S2	0.093	47.59	0.104	264.329	>1000	0.056	0.031
S3	0.004	0.006	23.676	>1000	>1000	0.128	0.02
S4	0.023	0.037	0.018	11.194	>1000	0.354	0.211
S5	0.005	>1000	>1000	>1000	>1000	0.156	0.024
S6	>1000	>1000	0.034	>1000	>1000	0.415	0.019
S7	585.05	>1000	>1000	4.113	>1000	0.073	0.064

Table 3.3: Savage-Dickey density ratios for Bayesian nested model selection in experiment 1. The header row indicates which point on the parameter space corresponds to the null hypothesis. Numerical values are the ratio of posterior and prior densities evaluated at the null point. Values larger than 20 are considered strong evidence against the null. The prior densities for each parameter are given in table 3.2. The prior density for difference parameter $\tau_{\text{same}} - \tau_{\text{oppo}}$ is constructed from the difference of two exponential random variables (i.e. a Laplacian random variable).

3.3 Experiment 2

In experiment 1, every stimulus was comprised of exactly 9 black dots and 9 white dots. While this equalized the chances of neighboring dots having the same or opposite polarities, it also introduced the possibility that our results in experiment 1 are due to this property. Experiment 2 was designed to investigate this issue.

3.3.1 Methods

The methods in experiment 2 were identical to experiment 1, except that half of the stimuli contained 13 black dots and 5 white dots; the remaining half contained 5 black dots and 13 white dots.

3.3.2 Model

The model in experiment 2 was identical to the model in experiment 1, except that the parameters τ_{same} and τ_{oppo} were replaced by τ_{many} and τ_{few}. Accordingly, this changed the function in equation 3.7 to 3.12.

$$z_d = \sum_{\substack{\text{dots } e \neq d \\ \text{with} \\ e \in \text{Few}}} f_{\text{few}}\left(\|v_e - v_d\|\right) \quad + \quad \sum_{\substack{\text{dots } e \neq d \\ \text{with} \\ e \in \text{Many}}} f_{\text{many}}\left(\|v_e - v_d\|\right) \tag{3.12}$$

where

$$f_{\text{few}}(q) = \cos^2\left[\frac{\pi}{4} + \rho\right] \exp\left[\frac{-q^2}{2\tau_{\text{few}}^2}\right] \quad \text{and} \quad f_{\text{many}}(q) = \sin^2\left[\frac{\pi}{4} + \rho\right] \exp\left[\frac{-q^2}{2\tau_{\text{many}}^2}\right]. \tag{3.13}$$

3.3.3 Results

Black dots exert slightly more weight than white dots

As shown in figure 3.8, the effect from experiment 1 is replicated for 2 of 3 subjects who participated in both experiments. Subject 3 shows the largest difference across experiments. For this subject, it appears the manipulation in experiment 2 ameliorates the systematic bias caused by darker regions in the display.

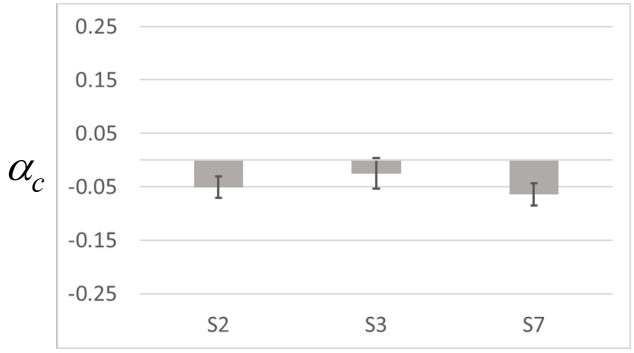

Figure 3.8: The parameters α_c for all subjects who completed experiments 1 and 2. Heights show posterior expectation. Error bars show 95% Bayesian credible intervals.

Peripherality exerts a significant influence whose direction varies across subjects

As shown in figure 3.9, the effect of dot peripherality remains significant for all subjects in experiment 2. For subjects 3 and 7, the direction and magnitude of the effect is about the same across both experiments. However, for subject 2, the direction of the effect is reversed.

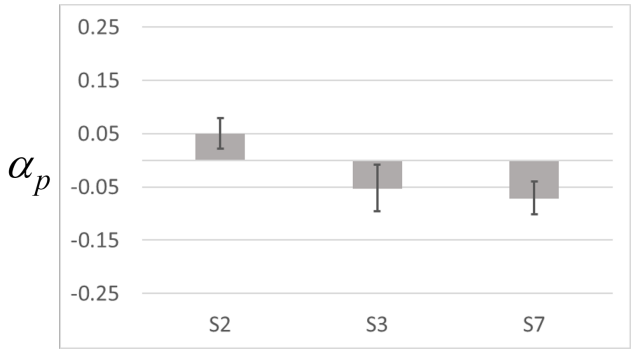

Figure 3.9: The parameters α_p for all subjects who completed both experiments 1 and 2. Heights show posterior expectation. Error bars show 95% Bayesian credible intervals.

Residual density exerts a strong negative influence on dot weights for all subjects

As shown in figure 3.10, the effect of residual density remains significant for all subjects in experiment 2. The direction and magnitude of the effect is preserved across both experiments, which suggests the effect observed in experiment 1 cannot be explained by the equal proportions of dot colors in each stimulus.

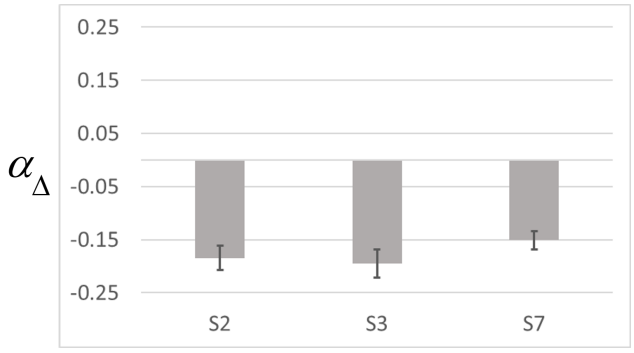

Figure 3.10: The parameters α_Δ for all subjects who completed experiments 1 and 2. Heights show posterior expectation. Error bars show 95% Bayesian credible intervals.

Spatial Additive Biases

As shown in figure 3.11, for all three subjects the expected value of β_x, β_y, or both is significantly different from 0. In all cases, however, they are also quite small. An interesting

change is observed in the additive biases for subject 2– it appears the vertical bias changed direction and increased in magnitude as a result of the manipulation in experiment 2.

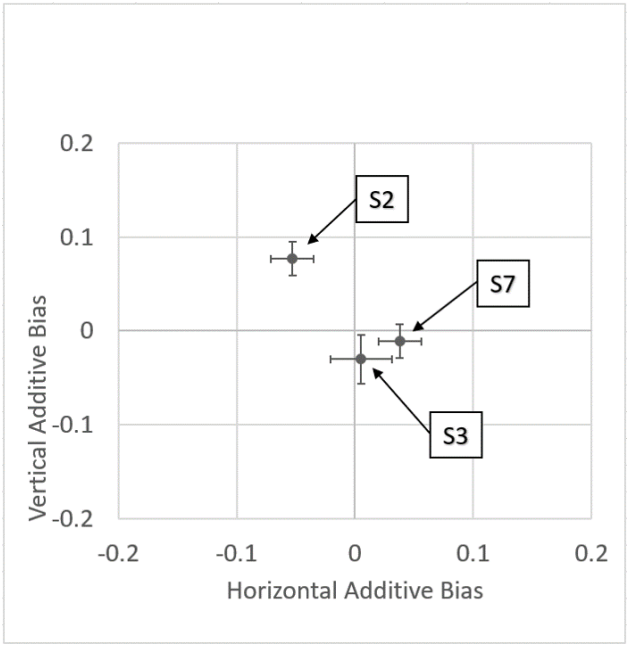

Figure 3.11: The parameters (β_x, β_y) for all subjects who completed experiments 1 and 2. Points show posterior expectations. Error bars show 95% Bayesian credible intervals.

The density of a dot's context.

A central question motivating this study was whether or not the density of the context for a given dot d was influenced similarly or different by dots of the same vs. opposite polarity to d *when the proportions differed across stimuli.* As shown in figure 3.12, the relative influence exerted on $z_{d,k}$ by dots of the same vs. opposite polarity and also in stimulus S_k is affected by the manipulation in experiment 2. The largest effect is seen in subject 2. For this subject, dots of the same polarity as d appear to exert greater influence than dots of the opposite polarity. For subjects 3 and 7, dots of the same polarity as d appear to exert less influence than dots of the opposite polarity.

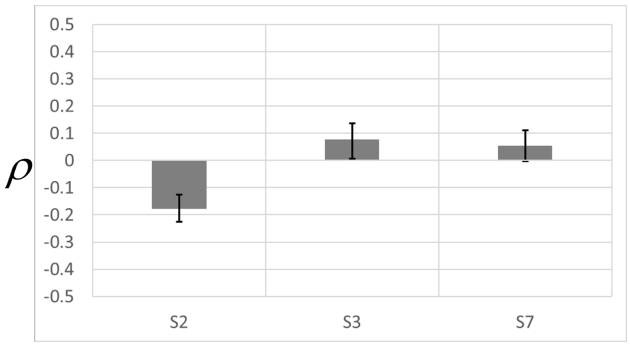

Figure 3.12: The parameter ρ for all subjects who completed experiments 1 and 2. Height of the bar shows posterior expectation. Error bars show 95% Bayesian credible intervals.

As shown in figure 3.13, for two of three subjects, the distance across which dots of the same vs. opposite polarity as d can influence $z_{d,k}$ is unaffected by the manipulation of experiment 2. For subjects 3 and 7, the credible intervals for both scale parameters τ_{few} and τ_{many} overlap, suggesting these parameters do not differ significantly. Furthermore,for subjects 3 and 7, the posterior expectations for τ_{few} (τ_{many}) are comparable to those for τ_{same} (τ_{oppo}). This suggests that the spatial scale over which subjects 3 and 7 aggregate information about the stimulus is not affected by the manipulation in experiment 2.

However, the manipulation in experiment 2 appears to affect subject 2. The credible intervals do not overlap, which suggests subject 2 aggregates information about the few group over a smaller spatial scale than the many group when the proportions differ across stimuli. Furthermore, the posterior expectations for τ_{few} (τ_{many}) are less than to those for τ_{same} (τ_{oppo}). This suggests the spatial scale over which subject 2 aggregates information about the stimulus is reduced by the manipulation in experiment 2.

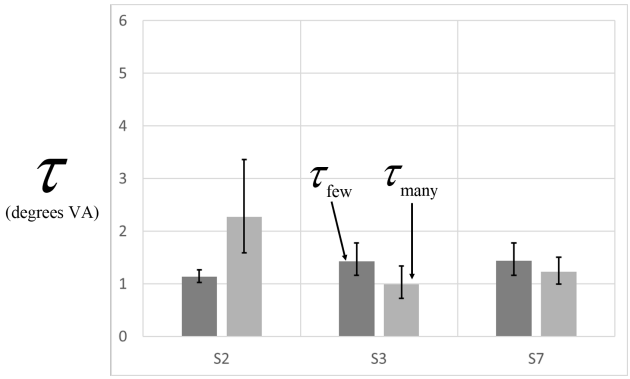

Figure 3.13: The parameters τ_{few} and τ_{many} for all subjects who completed experiments 1 and 2. Height of the bar shows posterior expectation. Error bars show 95% Bayesian credible intervals.

Model Selection

The results for parameters ρ, τ_{few}, and τ_{many} suggest the DPB model (in which the computation of $z_{d,k}$ is blind to polarities of all dots in the display) may fit the data was well as the full model for subjects 3 and 7, but not for subject 2. This is supported by the Save-Dickey density ratios for experiment 2, reported in table 3.4 Wagenmakers et al. (2010).

	$\beta_x = 0$	$\beta_y = 0$	$\alpha_c = 0$	$\alpha_p = 0$	$\alpha_\Delta = 0$	$\rho = 0$	$\tau_{\text{few}} - \tau_{\text{many}} = 0$
S2	>1000	>1000	>1000	5.308	>1000	>1000	90.633
S3	0.025	0.269	0.078	0.533	>1000	0.924	0.424
S7	177.294	0.048	>1000	>1000	>1000	0.391	0.077

Table 3.4: Savage-Dickey density ratios for Bayesian nested model selection in experiment 2. The header row indicates which point on the parameter space corresponds to the null hypothesis. Numerical values are the ratio of posterior and prior densities evaluated at the null point. Values larger than 20 are considered strong evidence against the null. The prior densities for each parameter are given in table 3.2. The prior density for difference parameter $\tau_{\text{few}} - \tau_{\text{many}}$ is constructed from the difference of two exponential random variables (i.e. a Laplacian random variable).

3.4 Discussion

Using a regression-like model of dot weights, it is possible to explain variations in systematic error using variation in hypothetical feature statistics. We used this modeling approach to show the sources of systematic bias can be broadly classified as obligatory or idiosyncratic. An obligatory bias is a source of error that is present in most, if not all, strategies chosen by a human subject and cannot be ameliorated with training (see figures 3.4 and 3.10). An idiosyncratic bias is a source of error that varies between subjects performing the same task (i.e. individual differences), or possibly between tasks performed by the same subject (see differences in figures 3.3 and 3.9 for subject 2).

Additional idiosyncrasies appear in the subjective density measures we modeled with equations 3.7 and 3.12. According to the model fits, there are minor individual differences in the scale of spatial aggregation (variability in τ from figures 3.7 and 3.13). It is interesting that most, if not all, subjects aggregate information over a spatial scale that is less than the dispersion of the stimulus. This is consistent with a process where locally-registered signals are pooled at successively larger scales, and not a process where an observer uses global parameters like dispersion to predict the target.

3.4.1 Estimation strategies are obligatorily biased by configurations of stimulus information

Two obligatory biases reported here are explained by contrast polarity and residual density.

3.4.1.1 Dark regions

Figure 3.2 shows most subjects' responses tend to gravitate more towards regions of the display that are darker than average, and figure 3.8 shows that the effect is not affected by the manipulation in experiment 2. The fact that most subjects are biased by color might seem surprising at first given the instructions to ignore color, but the effect has been reported using the centroid task (Drew et al., 2010). The obligatory bias towards darker elements in the stimulus is consistent with the previously reported blackshot effect (Chubb et al., 2004). It appears variations in luminance across space are more salient when the local intensity is less than average. While the effect size of this bias is small, it is significant for more than half our subjects. This suggests humans are limited in their capacity to ameliorate the effect through training.

3.4.1.2 Sparse regions

Figure 3.4 shows all subjects' responses tend to gravitate towards sparser regions of the display, regardless of the location, and figure 3.10 shows that this effect is not affected by the manipulation in experiment 2. In other words, the density effect persists for all subjects, despite being decorrelated with peripherality, and the idiosyncrasies that account for individual differences in estimation bias.

3.4.2 Estimation Strategies are idiosyncratically biased

Figure 3.3 shows the effect of peripherality varies across subjects, and figure 3.9 shows how the magnitude of the effect is affected by the manipulation in experiment 2 for two out of three subjects. Interestingly, the direction of the effect reverses for subject 2. Assuming the peripherality statistic is an accurate description of the true stimulus representation, this

suggests a degree of flexibility in the strategy chosen by some (but not all) human subjects. However, since the statistic was designed for linear decorrelation with the density statistic (and not chosen for accuracy), it remains possible that this trend reflects a failure of the model to capture the strategy deployed by subject 2.

3.4.3 Subjective density may be influenced by regularities in stimulus information

The manipulation in experiment 2 appears to change the density-related component of the strategy deployed by subject 2. In experiment 1, there is little-to-no evidence the full model is better than the DPB model (see table 3.3). Table 3.4 shows evidence for two changes in the perception of density for subject 2. First, the subject aggregates information about the more numerous group over a larger scale of space than the less numerous group. Second, dot clusters are subjectively more dense when they contain dots from the few group.

3.4.4 Implications for neurocomputational models of centroid estimation

Table 3.3 shows the DPB model fits the data at least as well as the full model, which suggests the type of neuron most likely responsible for the obligatory bias towards sparser regions of the display is a cortical complex cell. Table 3.4 shows this result is replicated in experiment 2 for most of the subjects who participated in both experiments.

The neural mechanism proposed by Moreland and Boynton (2017) can explain both obligatory biases reported here, but only if they occur at different levels of processing. For the obligatory bias towards darker regions to emerge from the response of a neuron saturating at higher intensities, the response should rise the most at 0 intensity and saturate completely

before intensity 1, without any discontinuities near the average intensity. Based on this description, the type of neuron most likely responsible for the obligatory bias towards darker regions of the display is a precortical simple cell.

Figures 3.7 and 3.13 show the spatial scale over which each subject aggregates information in order to generate a perceptual representation of local density. There is a trend– this scale parameter is less than true dispersion parameter used to generate the stimulus clouds. If humans aggregate information over a spatial scale that is, typically, half of the true dispersion parameter, this illustrates a principle of stimulus encoding that limits performance. How then are humans such efficient centroid estimators? The answer may depend on the availability of a convex pooling region, such as illusory contours or perceived boundary of a visual object. By inducing a binary partition of visual space into a convex set of possible target locations, it is possible to search for "the best" target through linear combinations of any subset points inside the convex region (i.e. all possible target locations).

3.4.5 Parametric Modeling Approach: Pros and Cons

Systematic biases either depend on features of the stimulus, or they do not. In chapter 2, we measured the estimation bias for each stimulus pattern (equation 1.9). In chapter 3, we investigate possible sources of bias in terms of some hypothetical feature statistics, and attempt to measure the influence of those quantities using a regression-like model of the dot weights. The benefits of this approach are the ability to explain the biases of a particular estimation strategy in terms of statistics that vary simultaneously between stimuli. Obviously this allows for more rapid inference than an approach like in ours in chapter 2. Furthermore, since the regression model in equation 3.3 can be used for any arbitrary set of statistics, this modeling approach could provide a way of comparing different statistics' ability to describe the subject's strategy.

The approach must be used with caution for at least two distinct reasons. First, if the feature statistics are not actually relevant to the subject's strategy, then inference is a bust. The nesting configurations provide one safeguard against this outcome, since in extreme cases the full model should perform no better than the fixed bias model, but it is not a perfect solution. Therefore the investigator must choose a set of feature statistics with extreme care, and use the smallest number possible. Second, as shown in figure 3.14, the most popular Frequentist approaches for nested model comparisons are not appropriate for deriving the distribution of likelihood ratio test statistics under the null hypothesis that the simpler model captures the true state of the world. This means that the difference in model parameters cannot be expressed in terms of independent linear constraints on data log-likelihood, or there is a violation of the independence assumption that justifies the approximation offered by Wilks (1944).

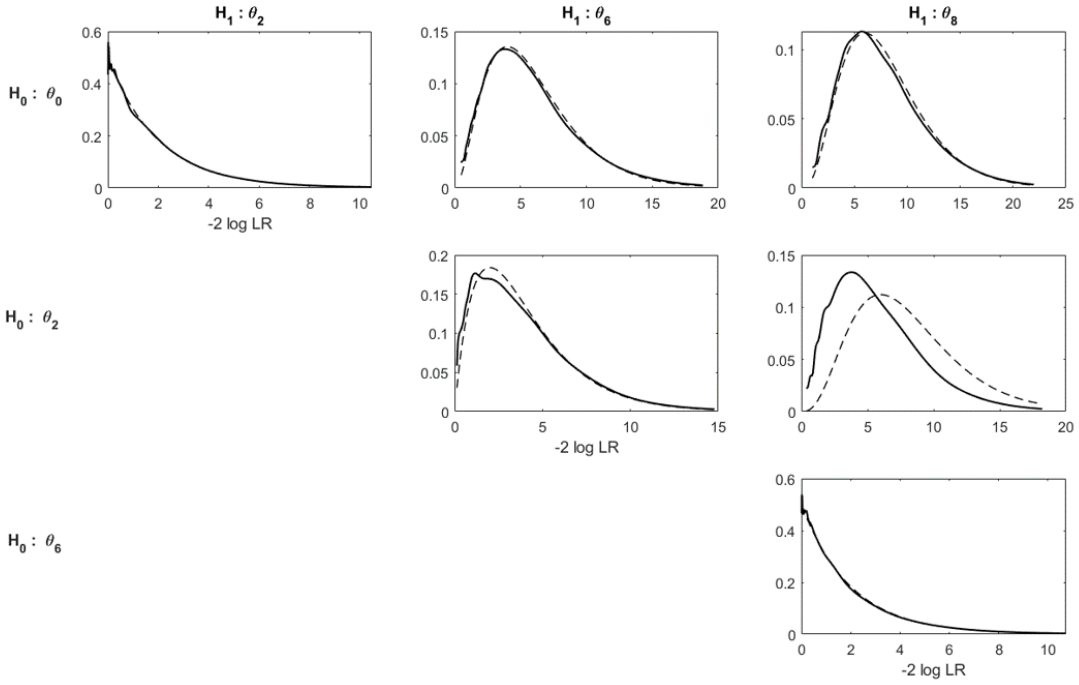

Figure 3.14: Distributions of the likelihood ratio test statistic constructed by simulation from our data (solid lines). According to Wilks (1944), assuming the simpler model captures the true state of the world, each of these should be a chi-squared distribution with degrees of freedom equal to the difference in free parameters (dotted lines). Each row of panels is for a different truth level, which is indicated to the left of all panels. Each column of panels is for a different alternative, which is indicated above all panels. Panels where the two lines are distinguishable indicate comparisons that require simulation.

In chapter 3, we took a Bayesian approach to model selection and verified our conclusions two ways. The first is by visual comparison of the credible intervals in the figures and plots. Using this method, differences are significant when the credible intervals do not overlap. The second is with Savage-Dickey density ratios in the tables. The Savage Dickey Density ratios are less likely to claim significant results than credible intervals. However, the density ratios are calculated under the assumption of independent marginals, where the credible intervals are not– therefore we argue the Savage-Dickey density ratios are more conservative, but the credible intervals provide a complete picture of the posterior dependencies.

For situations where the choice of priors is not obvious, we offer a third approach to model selection based on dependent samples t-test. First, we introduce a new quantity in equation 3.14.

3.4.5.1 Preliminaries

Let θ_0 and θ_1 represent two possible models, where $\theta_0 \subset \theta_1$ (i.e. θ_0 is nested within θ_1). Let P_0 (P_1) denote the dimensionality of θ_0 (θ_1). Further, recall the definitions of $\hat{\boldsymbol{\phi}}_k$ and $\boldsymbol{\varphi}(S_k;\theta)$ provided earlier (see equations 1.6 and 3.2).

$$D_k(\theta_0,\theta_1) = c_0\left\|\boldsymbol{\varphi}(S_k;\theta_0) - \hat{\boldsymbol{\phi}}_k\right\|^2 \quad - \quad c_1\left\|\boldsymbol{\varphi}(S_k;\theta_1) - \hat{\boldsymbol{\phi}}_k\right\|^2 \tag{3.14}$$

The constants c_0 and c_1 can be varied to optimize the power of the statistical test (under the constraint $1 < c_0 < c_1$). For initial values, we recommend the following:

$$c_0 = \frac{2K}{2K - P_0} \quad \text{and} \quad c_1 = \frac{2K}{2K - P_1}$$

3.4.5.2 New quantities

Now from K unique stimulus patterns, we obtain the sample statistic in equation 3.15.

$$\bar{D}(\theta_0, \theta_1) = \frac{1}{K} \sum_{k=1}^{K} D_k(\theta_0, \theta_1). \tag{3.15}$$

Which can be subjected to a t-test of the null hypothesis $H_0 \ : \ \mathrm{E}\big[D\big] = 0$. We use a right-tailed test because we never expect $\bar{D} < 0$ under the nesting configuration where θ_1 must be able to account for at least as much as θ_0. Figure 3.15 shows the power functions for this test and the Likelihood ratio test for the DPB model versus the full model, in a simulated experiment where the true value of ρ varies along the horizontal axis, and the true difference $\tau_2 - \tau_1$ is shown above the panel. In all cases, the test being performed is reflected in the bottom right panel of figure 3.14. The left panel illustrates the power functions when the null hypothesis can capture the true state of the world because the true difference $\tau_{\text{same}} - \tau_{\text{oppo}} = 0$. The right panel illustrates the power functions when the null hypothesis cannot capture the true state of the world the true difference $\tau_{\text{same}} - \tau_{\text{oppo}} \neq 0$. The performance of the t-test method is relatively unaffected by the small difference between scale parameters.

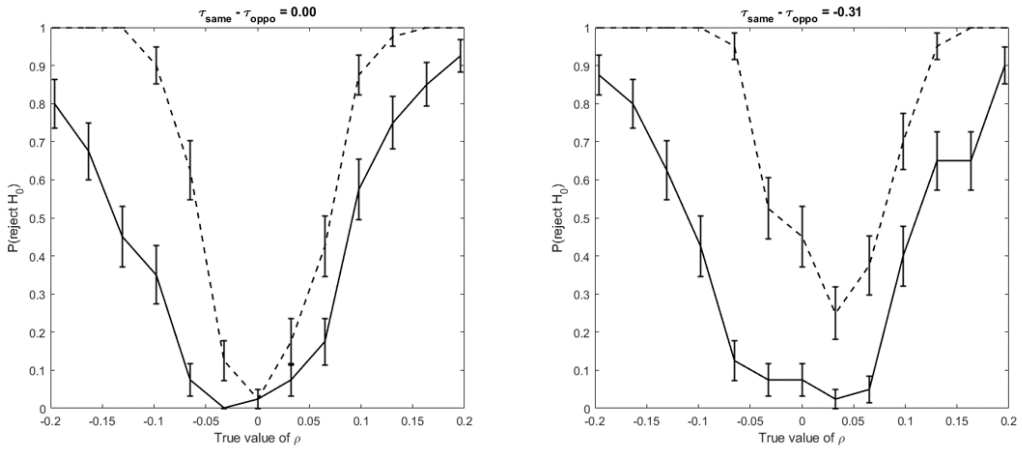

Figure 3.15: This figure illustrates the differences between the likelihood ratio test statistic (dotted line) and the t-test statistic (solid line)in terms of power functions. In both panels, the null and alternative hypothesis is test corresponding to the bottom right panel of figure 3.14, and the test is performed at the .05 level. The figure illustrates that the t-test method is more robust to small differences in τ_1 and τ_1.

Chapter 4

Investigations into estimation strategies with covert spatial attention

4.1 Introduction

Posner (1980) provides an experimental paradigm for measuring properties of spatial attention. This paradigm uses a transient symbolic cue presented to peripherally or foveally to direct exogenous or endogenous attention to a location in the visual field. A target is presented some time after the cue, and subjects perform an alternative forced-choice task to indicate the veracity of their target representation. On the majority of trials, the target is presented at the same location as the cue (i.e. cue is valid) It is critical that the target occasionally appears elsewhere (i.e. cue is invalid) because this allows researchers to infer the cost of inattention to the target location. By measuring the differences in performance statistics, this paradigm allows one to study spatial attention in terms of cue effectiveness across experimental conditions. The paradigm provides a coarse description of spatial attention because many trials are required to estimate the effects in each condition.

Posner's cuing paradigm resonates with a spotlight metaphor of spatial attention (Norman, 1968; Eriksen and Eriksen, 1974) . According to this metaphor, the mechanisms of attention operate by "illuminating" a closed subset of visual space. The size (but not necessarily the shape) of the illuminated region should have a degree of flexibility. Objects falling within the attended region are detected more readily, and their features are processed with greater sensitivity. Meanwhile, the abilities to detect and discriminate outside the attended region are impaired. Early speculations about the nature of this spotlight did not rule out the possibility that the magnitude of effects decline continuously with distance. However, due to the coarse description offered by the initial paradigm, early attempts to model the spotlight did so with a binary gating function (Reeves and Sperling, 1986). There is also experimental evidence from this period that opposes the spotlight metaphor in favor of theories based on perceptual grouping (Driver and Baylis, 1989).

In the 40 years since Posner (1980), many properties of visual attention have been documented using variations of visual search and centroid tasks. Generally, valid cues are found to enhance performance (i.e. facilitation), while invalid cues impair performance (i.e. inhibition). Among the experimental factors reported to cause differences in facilitation and inhibition are retinal eccentricity, stimulus onset asynchrony (SOA), and whether the cue elicits exogenous or endogenous attention (Golla et al., 2004; Hetley et al., 2014; Carrasco, 2011). The following two questions remain open in the literature:

1. What control, if any, do subjects have over the size and shape of the attentional spotlight?

2. How does performance of attentional process depend on time stimulus information is available, retinal eccentricity, and size of the target region?

The goal of this experiment is to measure differences in the estimation strategies caused by three factors of interest: (1) The duration of stimulus availability, (2) the size of the

attended region, and (3) retinal eccentricity of the attended region. The experimental design ensures that optimal estimation strategies necessarily entail selectively processing items located inside a closed sub-region of visual space.

4.2 Methods

4.2.1 Subjects

All methods were approved by the UC Irvine Institutional Review Board. 3 subjects (1 female) provided written consent to participate in the study. The ages ranged from 25 to 65. All subjects were students or faculty at the University of California, Irvine, with extensive experience in a variety of centroid tasks.

4.2.2 Materials

All sessions were completed on a Dell desktop running the Windows 7 Professional operating system. Stimuli were generated in custom MATLAB code, and displayed using Psychophysics Toolbox Brainard (1997). Responses were collected on discretized pixel coordinates using an optical mouse connected to the desktop via wired USB. Subjects' viewing distance was fixed at 60 centimeters using a chin rest. From this distance, All stimuli were displayed inside a circular region that was 28 degrees in diameter.

4.2.3 Procedure

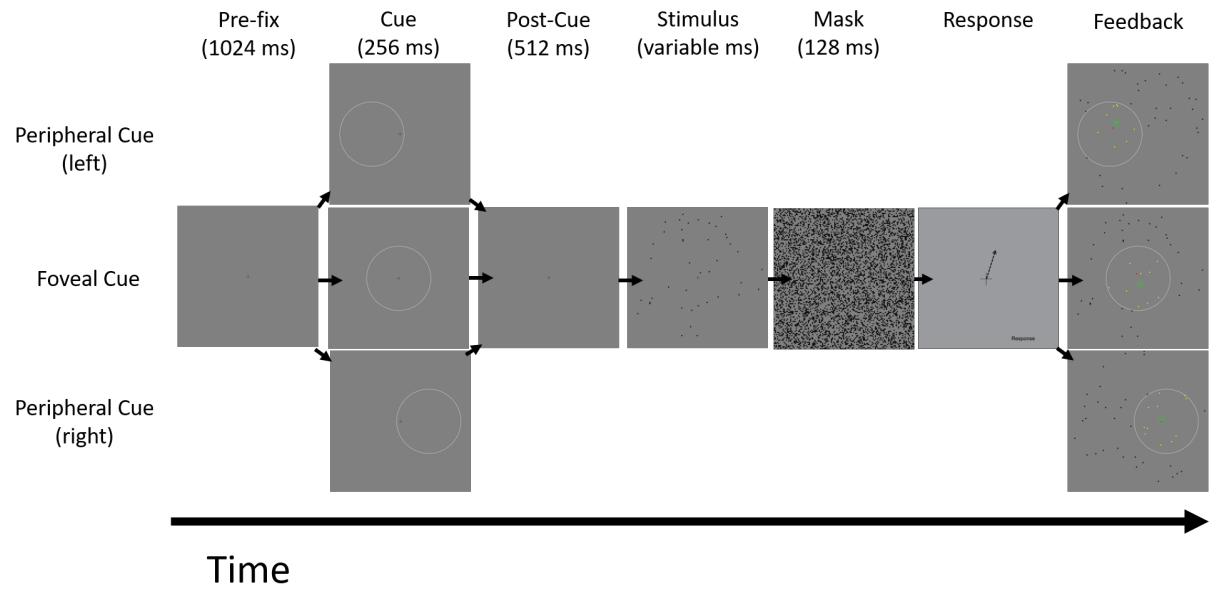

Figure 4.1: This figure illustrates the sequence of events in an experimental trial for chapter 4. Within a given block, the cued location varied randomly between three possible locations which are shown in separate rows.

The sequence of events on an given trial is illustrated in figure 4.1. After the subject initiated the trial, the events were as follows: The circular display with central fixation point for 1024 ms, followed by a spatial cue and central fixation point for 256 ms, followed by a central fixation for 512 ms, followed by a stimulus for either 64, 128, or 196 ms, followed by a mask for 128 ms. After this sequence, the subject provided a response, viewed feedback, and requested the start of another trial. The feedback display included (a) a modified version of the stimulus to highlight task-relevant components, (b) a green bullseye indicate the correct target location, and (c) a red dot indicating the observed response location. The subject was allowed to view this feedback for as long as desired before initiating the next trial.

Subjects were trained and trusted to maintain fixation on the central cross without an eye-tracker. Using an eye-tracker to abort trials where the instruction is not followed makes it impossible to guarantee the identical sequence of stimuli will be presented in both experimental sessions.

Each subject consented to three sessions. Each session consisted of 36 blocks of 54 trials, with a chance to rest in between blocks. The first session was training, and the second two sessions were experimental sessions where the subject responded to an identical sequence of stimuli twice. For a given subject, experimental sessions began around the same time of day as the training. To ensure consolidation of learned strategies during sleep, experimental sessions were scheduled at 24-48 hours after training, and both experimental sessions were scheduled no more than 3 days apart. Each session, the subject performed the same task under 18 experimental conditions (see table 4.1).

4.2.4 Stimuli

In any condition, a stimulus is comprised of a cued region, a random dot cloud, and a target location. All events were presented on a mean gray background (15.63 cd/m^2). We describe each of these now.

Cues to attend spatial regions

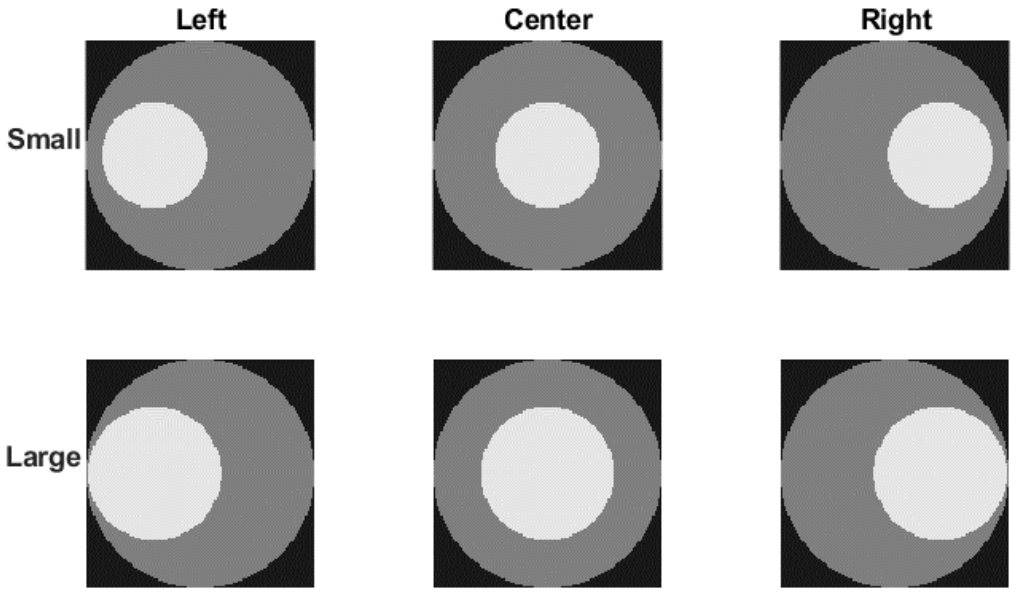

Figure 4.2: This figure shows the 6 regions of space cued during the experiment. The top row of panels is for the smaller cue conditions. The bottom row of panels is for the larger cue conditions. In each panel, the lighter regions indicate possible dot locations, and the lightest of these regions indicate possible target locations. In every experimental condition, the optimal strategy is to apply a filter that is uniform over the lightest region, and zero everywhere else.

In a block of trials, cues for covert spatial attention appeared 18 times at each of three possible locations in a random order (see second column of figure 4.1). Figure 4.2 shows the six spatially cued regions varying in location and size throughout the experiment. The cue persisted for 256 ms, followed by a 512 ms interval before the onset of the dot cloud. Therefore, subjects had at least 768 ms to deploy covert attention to the cued region before any information about dots became available. The border of the cue was lighter than the background (Weber contrast .56), and the interior was the same as the background.

Random dot clouds

Every dot cloud was generated by sampling (without replacement) 42 locations from the circular region of a 128-by-128 grid (see the not black regions of displays in figure 4.2). The locations on this grid were spaced to avoid overlapping dots in the stimulus. Only $12,892$ of the $16,384$ pixel locations on this grid were possible dot locations. The distribution of dot locations closely approximates a uniform distribution inside the circular region. When displayed to the subject, the diameter of these active locations subtended 28 degrees of visual angle. When displayed to the subject, each dot in the stimulus was a disc subtending 0.2 degrees of visual angle, with a Weber contrast very near -1.

If none of the sampled locations fell inside the cued region, the entire dot cloud was discarded and sampled again. Since the number of dots falling inside the cued region is a binomial random variable with rate parameter determined by the area of the cued region (see figure 4.3), it is simple to control the rate of discarded stimuli. We kept ours well below .05.

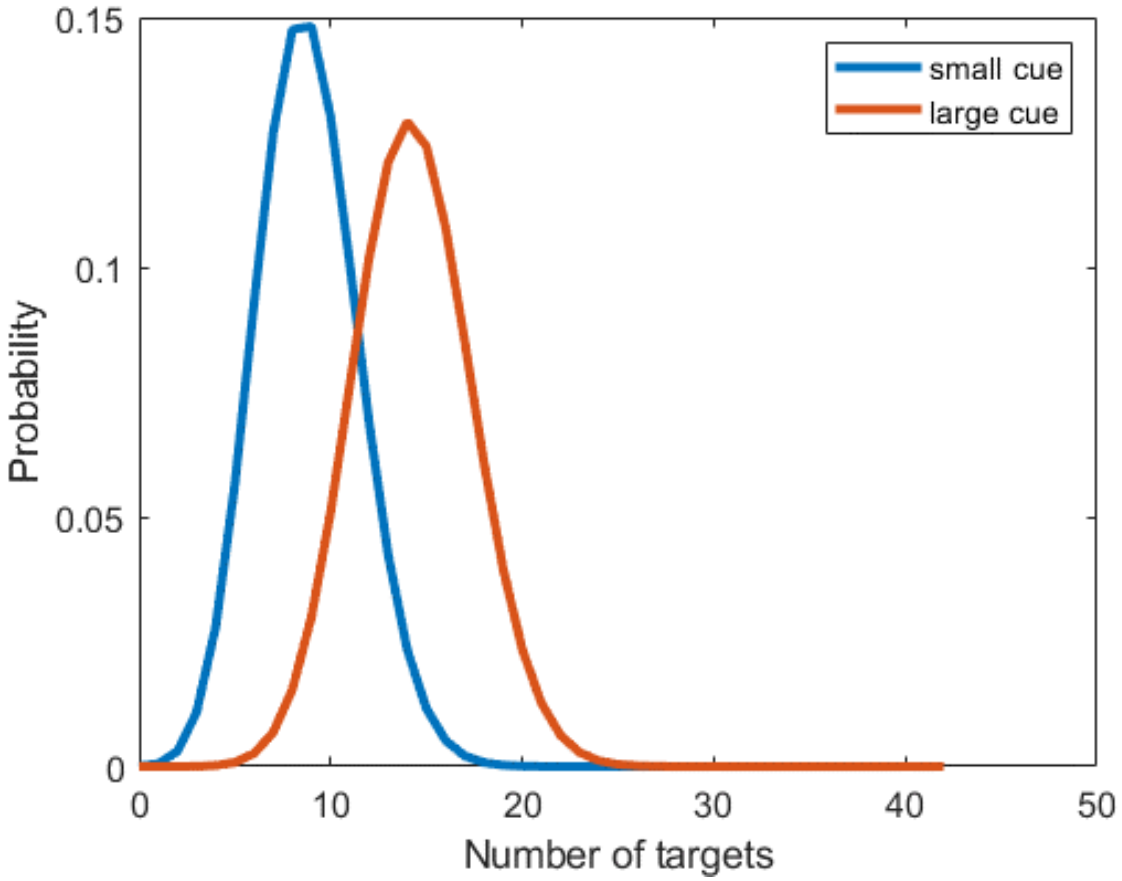

Figure 4.3: This figure shows the binomial probability distributions over the number of targets subjects could encounter in any given trial for small (blue line) and large (orange line) cue conditions.

Target locations

We write (C_x, C_y, C_r) for spatial location and radius of a cue. In chapter 3, the target location is a function of the optimal filter, defined in equation 4.1.

$$f_{\text{opt}}(x, y) = \begin{cases} 1 & \text{if } \sqrt{\left(x - C_x\right)^2 + \left(y - C_y\right)^2} < C_r \\ 0 & \text{otherwise} \end{cases} \tag{4.1}$$

4.3 Conditions

The experimental design uses 18 conditions generated from the 3 factors of interest (see table 4.1). We were primarily interested in how a given subject deploys covert spatial attention to a random location when attended regions and critical times vary in size and duration. For this reason, we kept the latter two factors fixed within any block of trials, but allowed the location of the cue to vary within each block.

The three levels of our stimulus duration factor were 64 ms, 128 ms, and 196 ms. If a critical time interval were defined from the onset of the cue to half way through the dot cloud exposure, those time intervals would be 800 ms, 832 ms, and 864 ms. Previous research suggests human subjects are able to deploy visual attention within all three durations.

We used two cue sizes to vary the area of the attended region. In the large cue conditions, the radius of the cued region subtended 7.54 degrees of visual angle, and covered approximately 34 percent of possible dot locations. In the small cue conditions, the radius of the cued region subtended 5.93 degrees of visual angle, and covered approximately 21 percent of possible dot locations. Figure 4.3 illustrates the difference between these conditions in terms of the number of target dots contained in a given stimulus.

condition	location of attended region	stimulus duration	size of attended region
1	left	64	small
2	left	64	large
3	left	128	small
4	left	128	large
5	left	192	small
6	left	192	large
7	center	64	small
8	center	64	large
9	center	128	small
10	center	128	large
11	center	192	small
12	center	192	large
13	right	64	small
14	right	64	large
15	right	128	small
16	right	128	large
17	right	192	small
18	right	192	large

Table 4.1: This table shows the 18 experimental conditions generated from 3 factors of interest. Within a given block, factors in the last two columns were fixed, and only the location of the cue was allowed to vary.

4.4 Model

4.4.1 The functional form of the attentional spotlight

Our model of spatial attention describes the surface of an influence function with 5 parameters. The model of spatial attention is for chapter 4 is defined in equation 4.2.

$$f(x,y) = \exp\left[-\left(\frac{(x-\mu_x)^2}{\alpha_x^2} + \frac{(y-\mu_y)^2}{\alpha_y^2} \right)^{\kappa/2} \right] \tag{4.2}$$

This is the kernel for a generalized bivariate Gaussian distribution. The height of this surface provides the unnormalized weight for any dot in the display as a function of its position in space. The peak location of this surface occurs at spatial coordinate (μ_x, μ_y), the steepness of the falloff in all directions in controlled by κ, and the pair of scale parameters (α_x, α_y) introduce directionally-dependent variations in size and shape.

4.4.2 The full response-production model

The parametric estimator for $\boldsymbol{\phi}(S_k)$ is defined in equation 4.3. The parametric estimator for chapter 3 uses the function in equation 4.2 plus an additional 3 parameters for components of the strategy that are based on prior beliefs instead of stimulus information.

$$\boldsymbol{\varphi}(S_k;\theta) = w_0 \begin{bmatrix} x_0 \\ y_0 \end{bmatrix} \quad + \quad (1-w_0) \sum_{d=1}^{42} w_{d,k} \begin{bmatrix} x_{d,k} \\ y_{d,k} \end{bmatrix} \tag{4.3}$$

Where the normalized weight $w_{d,k}$ is obtained from equation 4.2 via:

$$w_{d,k} = \frac{f(x_{d,k}, y_{d,k})}{\sum_{j=1}^{42} f(x_{j,k}, y_{j,k})}$$

The parameter pair (x_0, y_0) are default locations that anchor the strategy to the same location regardless of S. The parameter w_0 describes the strength of this anchor relative to the strength of available stimulus information.

The model uses a final parameter, σ^2, to describe residual error variance.

4.5 Results

4.5.1 Model-free measures of performance

Figures 4.4 and 4.5 show the systematic and random error components across experimental conditions for all three subjects. According to the mean-squared error decomposition from equation 1.5, estimates of these quantities are statistically independent. Thus, we can draw psychophysical inferences from each without considering the other. The figures show few trends across subjects, which suggests a degree of heterogeneity in the chosen estimation strategies. The following are five notable exceptions:

1. Systematic error magnitudes tend to be larger than random error magnitudes.
2. The magnitudes of systematic and random error are positively correlated.
3. The size of the attended region has a larger effect on random error than systematic error.
4. The duration of stimulus information has a larger effect on systematic error than random error.

5. Most detectable effects interact with location-by-subject.

4.5.1.1 Systematic error magnitude

Figure 4.4 shows the component of estimation error explained by systematic error. These values correspond to the square-root of the first term in the decomposition of equation 1.5. Variation in systematic error should be explained by defects in the chosen estimation strategy.

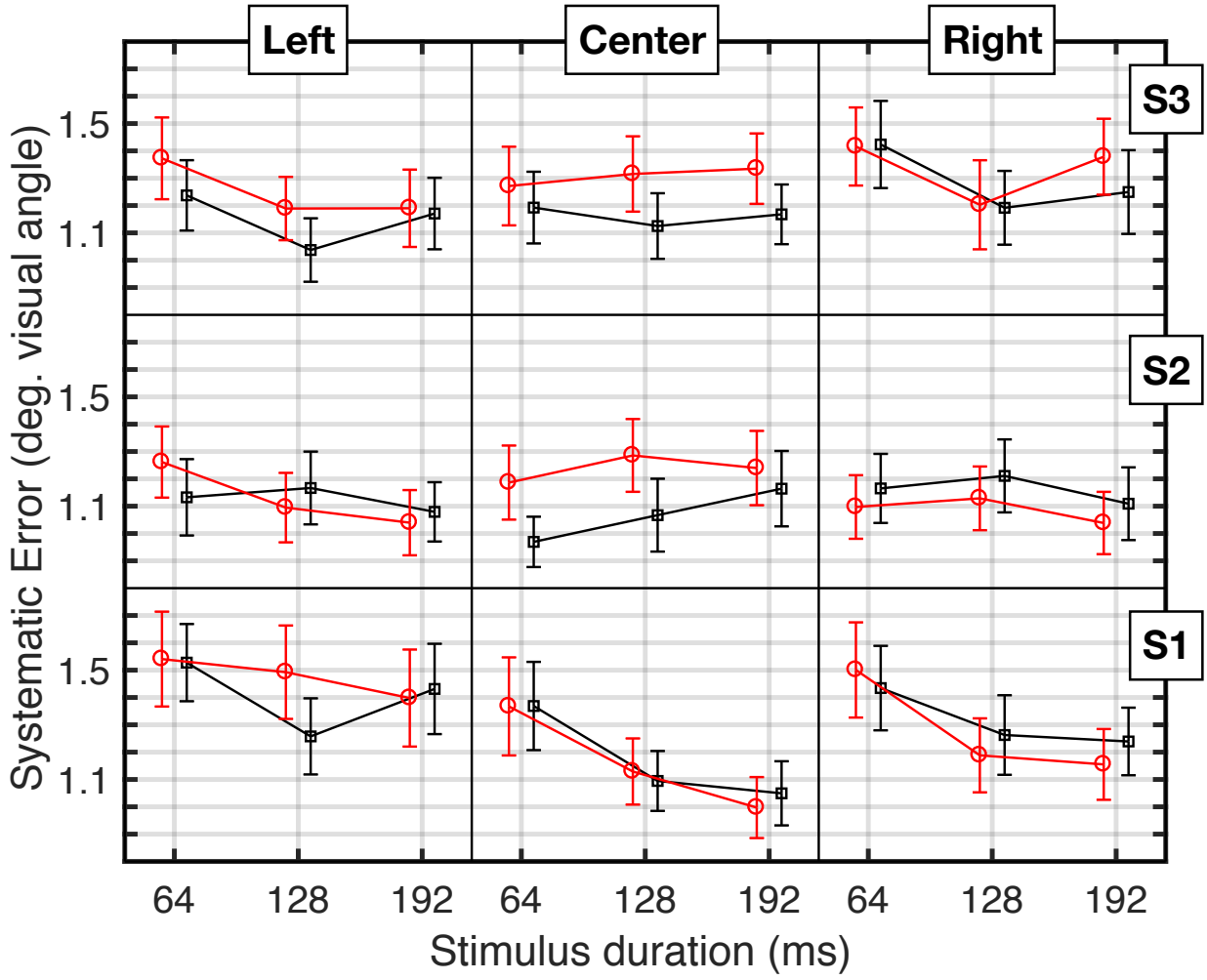

Figure 4.4: This figure shows how the systematic component of estimation error varies across levels of stimulus duration. Results for each subject (location) are shown on a different row (column). Results for small (large) cues are shown in black (red) lines. Expectations and confidence intervals are estimated from calculating the magnitude of 1.9 for all stimuli presented to a given subject and condition.

Subject 1 shows an effect of location. For subject 1, systematic error magnitudes tend to be largest when attending to the left periphery, intermediate when attending to the right periphery, and smallest when attending to the fovea. The apparent difference between left and right peripheries suggests the presence of hemispheric asymmetries.

Subjects 2 and 3 show location-dependent effects of cue size. For subject 2, systematic error magnitudes tend to increase with cue size when attending to the fovea, decrease with cue size when attending to the right periphery, but not in the left periphery. For subject 3, systematic error magnitudes tend to increase with cue size when attending to the left periphery and the fovea, but not in the right periphery.

Subjects 1 and 2 show location-dependent effects of stimulus duration. For subject 1, systematic error magnitudes tend to decrease with stimulus duration when attending to the when attending to the fovea or right periphery, but not in the left periphery. For subject 2, systematic error magnitudes tend to decrease with stimulus duration in the periphery, and increase with stimulus duration in the fovea.

4.5.1.2 Random error magnitude

Figure 4.5 shows the component of estimation error explained by random error. These values correspond to the square-root of half the second term in the decomposition of equation 1.5.

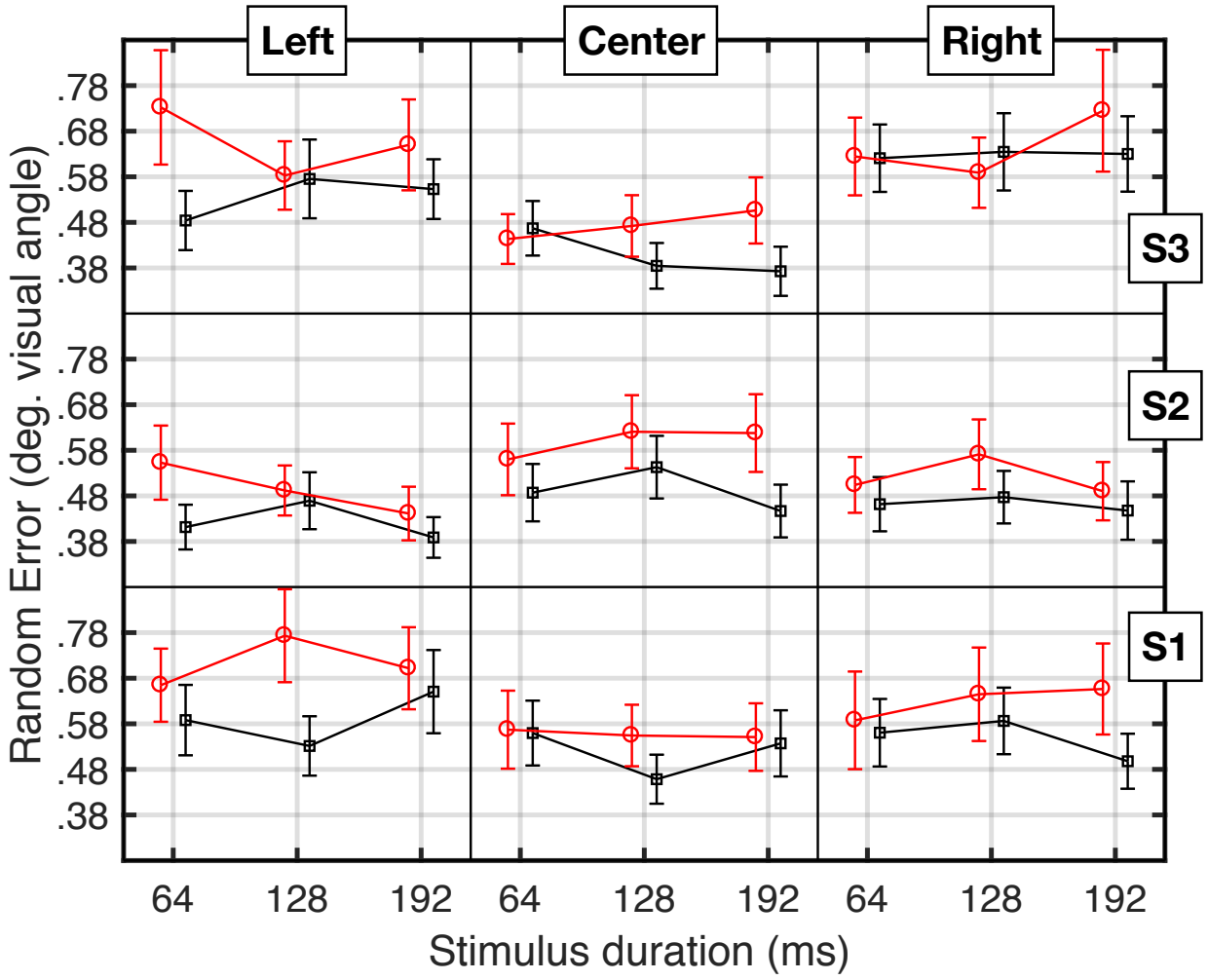

Figure 4.5: This figure shows how the random component of estimation error varies across levels of stimulus duration. Results for each subject (location) are shown on a different row (column). Results for small (large) cues are shown in black (red) lines. Expectations and confidence intervals are estimated from calculating the square root of 1.8 for all stimuli presented to a given subject and condition.

Most of the variation in random error magnitudes can be explained by the positive correlation with systematic error magnitude. Effects that are not explained by this relationship are described below.

All subjects show an effect of cue size. With some location-dependent exceptions (e.g. subject 3 attending to the right periphery), random error magnitudes tend to increase with the size of the attended region.

4.5.2 Model diagnostics

Before using the model to draw psychophysical inferences, it is important to determine how successfully the model fit the data, and if this success varies systematically. Ideally, the model should work reasonably well for all subjects, and for any given subject, should achieve roughly the same level of success in all conditions. If one of the factors systematically influences the success of the model, then the model should be reconsidered.

Below we present a quantity for diagnosing the model performance by comparing residual noise magnitude to the value expected from the model-free estimate of noise defined in equation 1.8, and illustrated in figure 4.5.

4.5.2.1 Random error ratio

If $\sigma_{\text{doublepass}}$ denotes an estimate of σ from the quantity defined in equation 1.8, and σ_{noise} denotes an estimate of σ from residual error of the model, then the random error ratio (RER) is a statistic defined in equation 4.4.

$$\text{RER} = \frac{\sigma_{\text{doublepass}}}{\sigma_{\text{noise}}} \tag{4.4}$$

This statistic can only take values in the interval $[0, 1]$. As the RER approaches 1, the model fit approaches perfection. Values larger than .5 are considered reasonable.

Figure 4.6 shows posterior expectations and 95% credible intervals obtained from MCMC sampling of the denominator in equation 4.4, while the numerator is fixed to the value estimated from data according to equation 1.8.

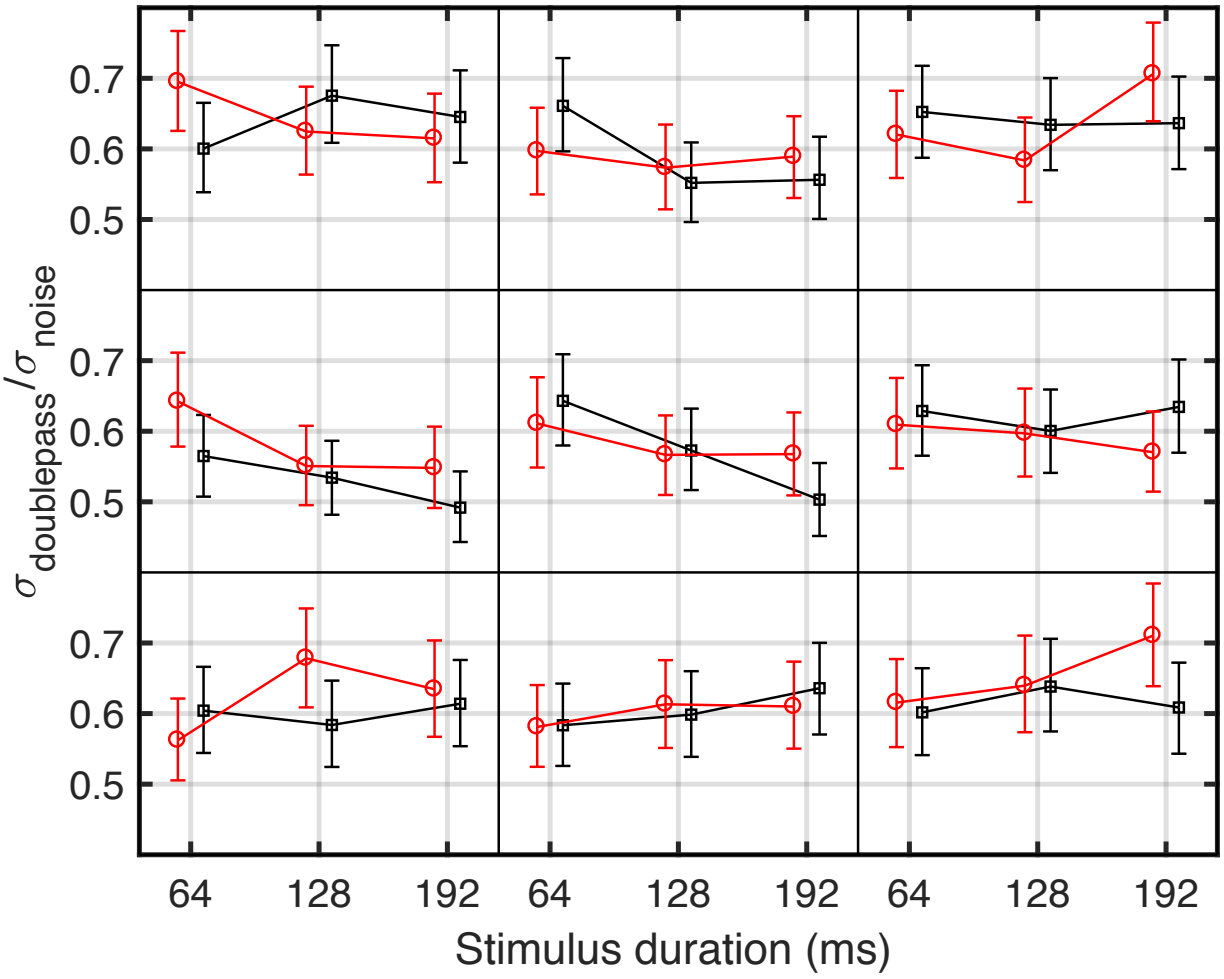

Figure 4.6: This figure shows how the random error ratio varies across levels of stimulus duration. Results for each subject (location) are shown on a different row (column). Results for small (large) cues are shown in black (red) lines. Posterior expectations and 95% credible intervals are estimated by MCMC.

According to the figure, the model provides a reasonable fit in all conditions for subjects 1 and 3. For subject 2, however, there appears to be structure in the data the model fails to

capture. The success of the model appears to decrease with stimulus duration, but only for subject 2 attending to the fovea or left periphery.

4.5.3 Model-based measures of performance

4.5.3.1 Suboptimality (mismatch to optimal filter)

The function f can be used to produce an image of attention distributed over space. By linearly transforming each pixel location (x, y) to $(\frac{x-C_x}{C_r} , \frac{y-C_y}{C_r})$, we obtain an image shifted to the cue center (C_x, C_y) and scaled to unit distance of C_r pixels. This is how the images in figure 4.7 were produced.

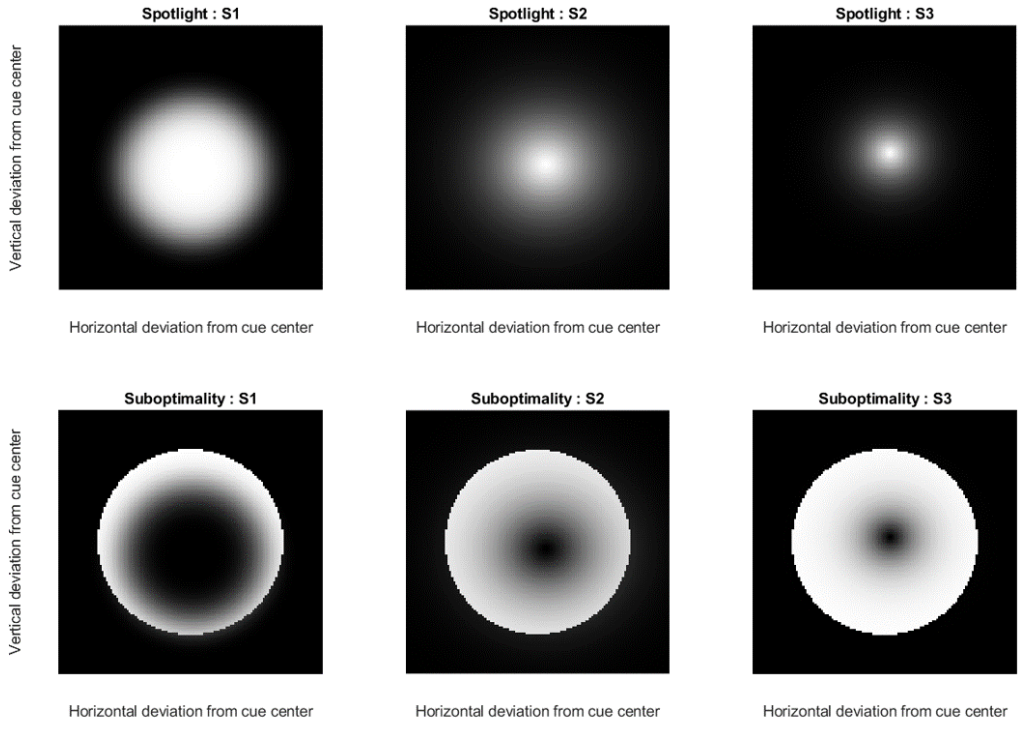

Figure 4.7: The top row in this figure shows spotlights for each subject, obtained from posterior expectations taken from data pooled over conditions where mean data-drivenness exceeds 1/2. The bottom row of this figure shows which regions of space deviate the most from the optimal filter from equation 4.1. Locations are shifted to the center of the cue, and scaled so the width of each panel is $\sqrt{2}$ times the diameter of the cue.

The top row of panels in figure 4.7 illustrates the spotlight each subject is expected to achieve in conditions where data drivenness exceeds 1/2. The bottom row of panels illustrates how every point in space contributes to suboptimal performance. There are substantial differences between subjects, which at least partially explains the individual differences shown in figure 4.4.

In order to obtain a performance statistic from these images, the area under the surface f (i.e. the amplitude) must be bounded. The expression in equation 4.5 is the chi-squared distance between two probability distributions, $P(x, y)$ and $Q(x, y)$. This is a measure of dissimilarity, which can provide a model-based measure of performance when P is a normalized estimate of the subject's spotlight and Q is the normalized optimal spotlight for the same condition. When the distance is zero, the estimated spotlight is optimal. As the distance increases, the data-driven component of systematic error is explained by the mismatch between achieved and optimal distribution of spatial attention.

$$D_{\chi^2}(P, Q) = \sum_{\forall (x,y) \in \text{ display}} \frac{\big(P(x, y) - Q(x, y)\big)^2}{P(x, y) + Q(x, y)} \tag{4.5}$$

Figure 4.8 shows the posterior expectation for this statistic, along with 95% percent credible intervals, for conditions where mean data-drivenness exceeds 1/2. It appears that regardless of the subject or condition, when the capacity to achieve the optimal strategy is measured this way, the limit is somewhere between 1/8 and 3/8.

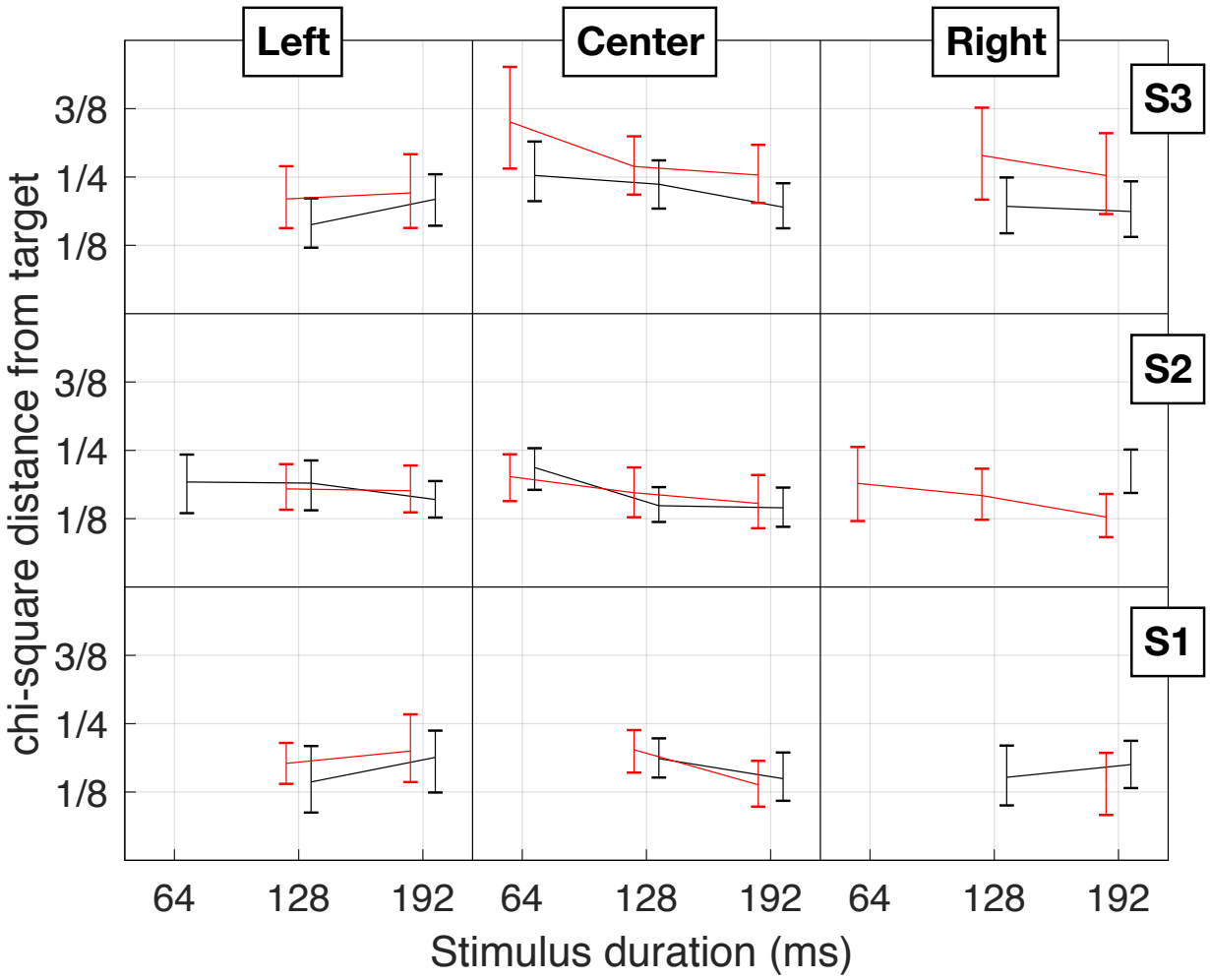

Figure 4.8: This figure shows how the suboptimality statistic from equation 4.5 varies across levels of stimulus duration. Results for each subject (location) are shown on a different row (column). Results for small (large) cues are shown in black (red) lines. Posterior expectations and 95% credible intervals are estimated by MCMC.

All subjects show a location-dependent effect of stimulus duration. All subjects are able to achieve a more optimal spotlight as stimulus duration increases, but only when attending to the fovea.

Subject 3 shows an effect of cue size. Subject 3 is able to achieve a more optimal spotlight when attending to smaller regions of the display.

4.5.4 Model-based explanations for estimation error

The suboptimality statistic defined in equation 4.5 and illustrated in figure 4.8 does not provide much information about which aspects of the strategy are responsible for estimation errors. However, by examining the estimated model parameters directly, it is possible to explain the estimation errors in more precise terms.

4.5.4.1 Data-drivenness

The parameter $(1 - w_0)$ from equation 4.3 is commonly called "data-drivenness" because it describes the extent to which the estimation strategy depends on knowledge of the dots in stimulus. When data-drivenness is high, the estimation biases are more easily explained by mechanisms of encoding/decoding dots in the stimulus. When data-drivenness is low, the estimation biases are more easily explained by an attraction to the default location (x_0, y_0). In the most extreme cases, as data-drivenness approaches 0 from the right, the parameters for equation 4.2 become unconstrained (conversely, as data-drivenness approaches 1 from the left, the default locations (x_0, y_0) from equation 4.3 become unconstrained).

Figure 4.9 shows posterior expectations for $1 - w_0$ with 95% credible intervals.

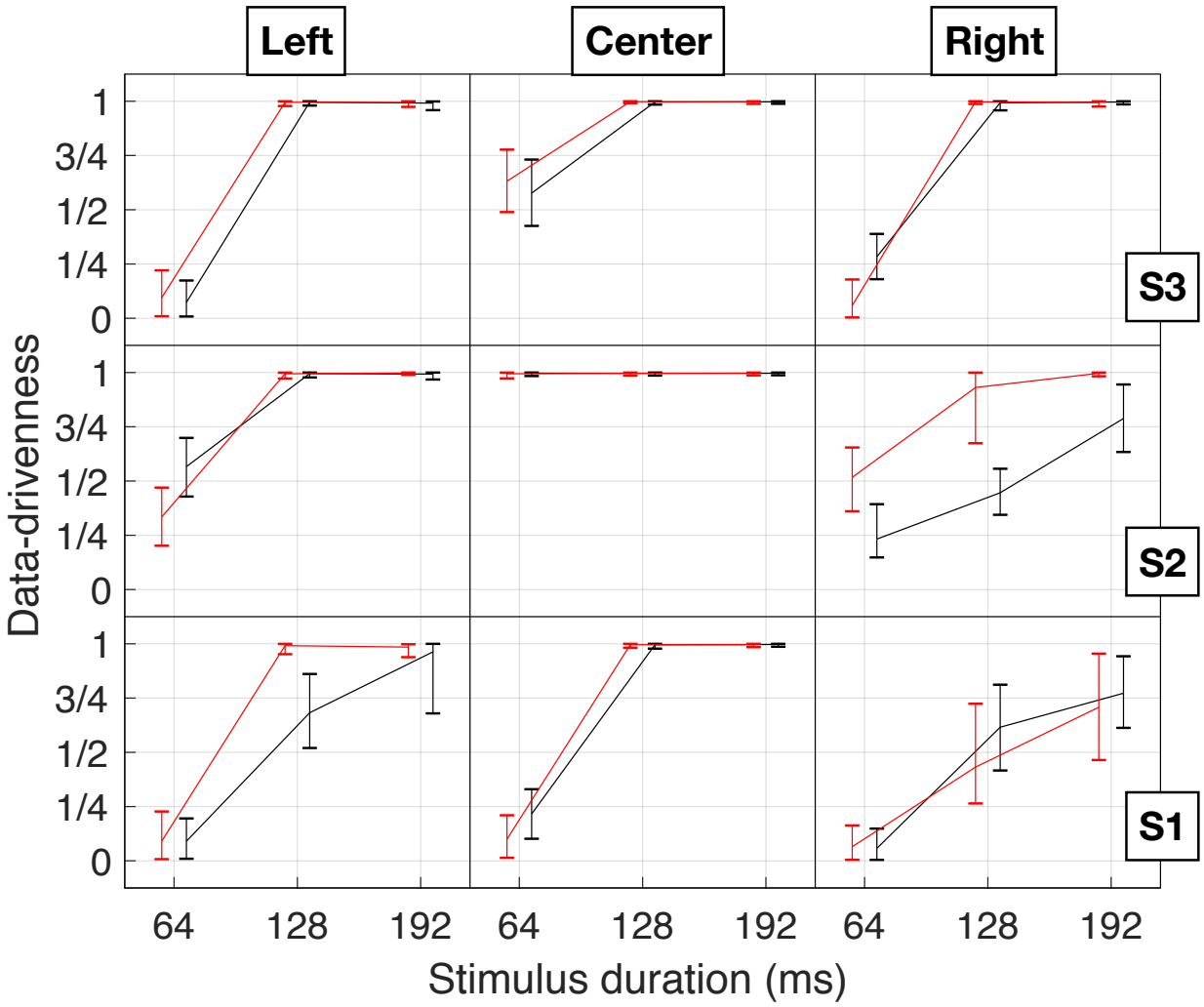

Figure 4.9: This figure shows how data-drivenness varies across levels of stimulus duration. Results for each subject (location) are shown on a different row (column). Results for small (large) cues are shown in black (red) lines. Posterior expectations and 95% credible intervals are estimated by MCMC.

All subjects show an effect of stimulus duration. Estimation strategies tend to become more data-driven as the stimulus duration increases.

All subjects show an effect of location. Estimation strategies tend to become more data-driven when attending to the fovea, compared to either side of the periphery. Furthermore, subjects 1 and 2 show evidence of the same peripheral asymmetry– strategies tend to be more data-driven in the left periphery.

All subjects show a location-dependent effect of stimulus duration. Estimation strategies tend to be more data-driven at shorter stimulus durations when attending to the fovea.

Subjects 1 and 2 show location-dependent effects of cue size. For subject 1, data-drivenness tends to increase with the size of the attended region, but only in the left periphery. For subject 2, data-drivenness tends to increase with the size of the attended region, but only in the right periphery.

4.5.4.2 Uniformity of attentional spotlight

The parameter κ from equation 4.2 is a measure of how volume under the spotlight is distributed over space. Using this measure, we can compare uniformity across conditions. When the value of this parameter is 2, the distribution is normal. For values less than 2, a larger proportion of the volume is concentrated in the tails (i.e. higher-than-normal kurtosis). For values larger than 2, a larger proportion of the volume is concentrated in the center (i.e. lower-than-normal kurtosis). In particular, as the value increases beyond 2 without bound, the volume becomes uniformly distributed between $[\mu_x - \alpha_x, \mu_x + \alpha_x]$ (horizontally) and $[\mu_y - \alpha_y, \mu_y + \alpha_y]$ (vertically).

Figure 4.10 shows posterior expectations and 95% credible intervals for this parameter in conditions where mean data-drivenness exceeds 1/2.

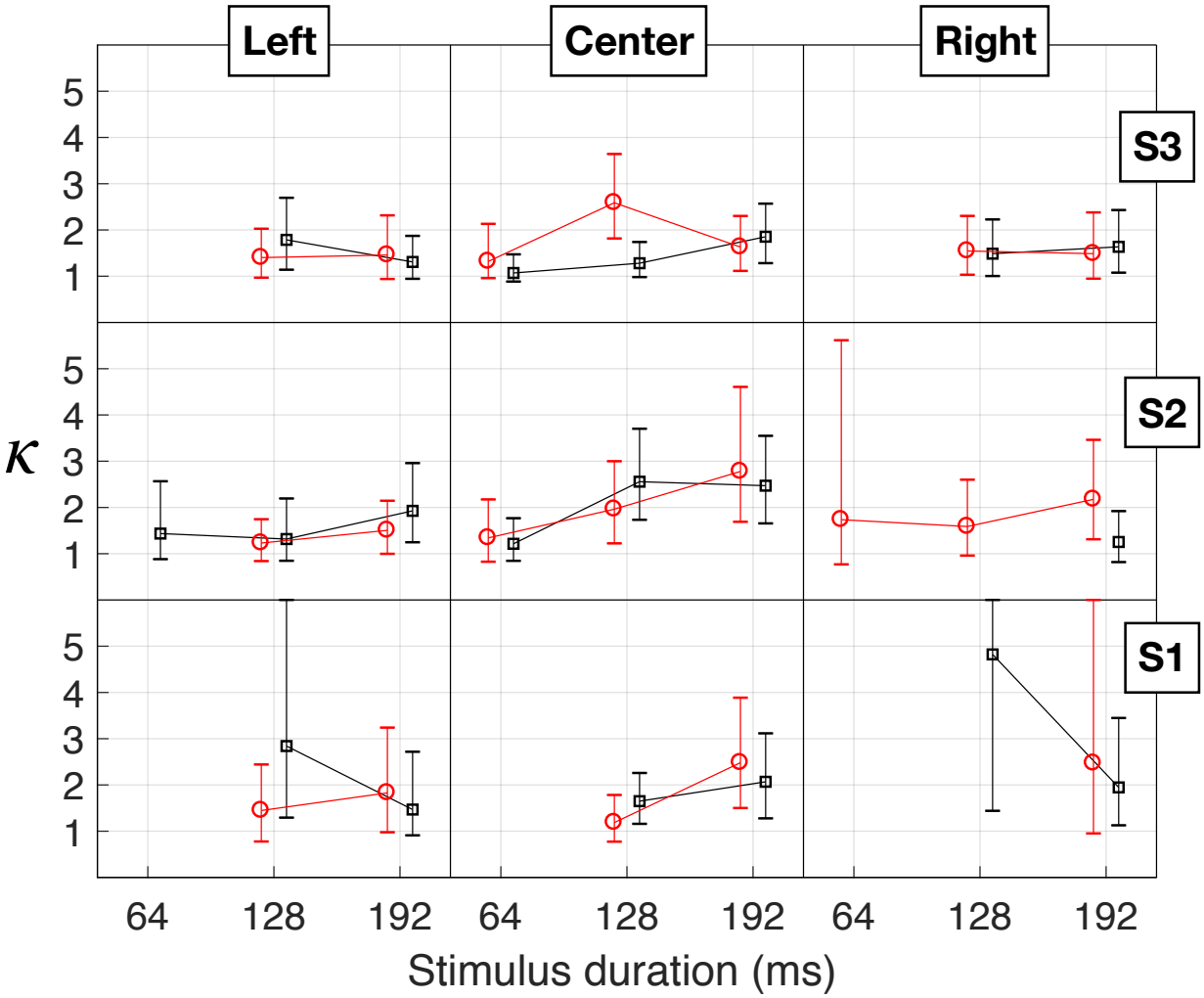

Figure 4.10: This figure shows how uniformity of the attentional spotlight vary across levels of stimulus duration. Results for each subject (location) are shown on a different row (column). Results for small (large) cues are shown in black (red) lines. Posterior expectations and 95% credible intervals are estimated by MCMC.

Subject 3 shows a location-by-size dependent effect of stimulus duration on the kurtosis. For subject 3, the volume of the spotlight follows a distribution with higher-than-normal kurtosis, but only for smaller cues centered on the fovea and at shorter stimulus duration.

For subject 1, the volume of the spotlight follows a distribution with higher-than-normal kurtosis only in the condition where large cues are centered on the fovea and the stimulus duration is 128 ms.

Importantly, none of the subjects are able to achieve uniform spotlights (i.e. $\kappa \gg 8$), which is necessary for optimum performance within the attended region.

4.5.4.3 Locus of attentional spotlight

If subjects directed the locus of attention to a location other than the cue, then we could explain some estimation error by the distance between (μ_x, μ_y), the spotlight center, and (C_x, C_y), the center of the cue. On the other hand, if $\mu_x = C_x$ and $\mu_y = C_y$, then the locus of attention is optimal, and we cannot explain estimation errors by subjects attending to the wrong location.

Figures 4.11 and 4.12 show posterior expectations and 95% credible intervals for these deviations in conditions where mean data-drivenness exceeds 1/2.

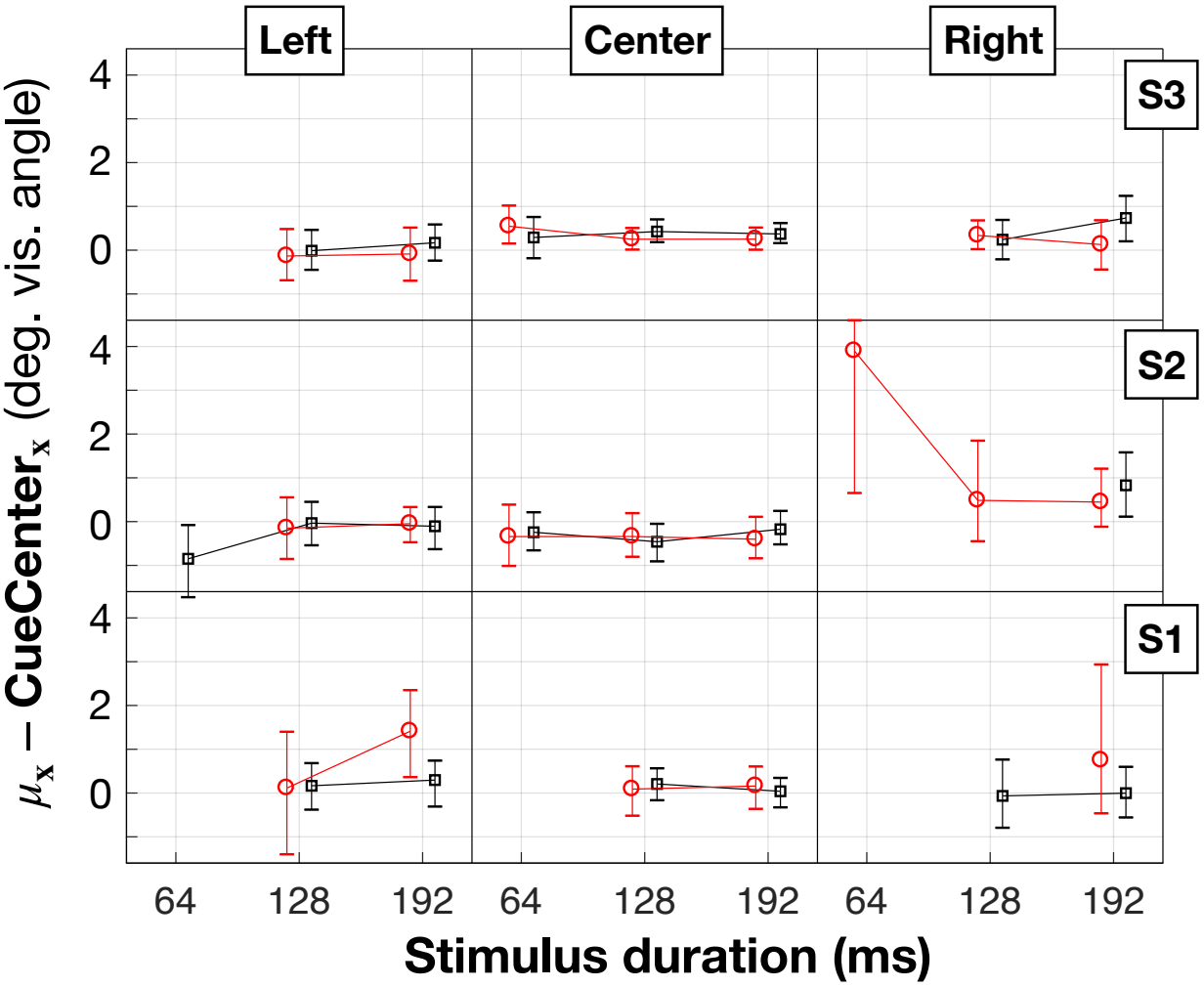

Figure 4.11: This figure shows how horizontal deviations of the attentional locus vary across levels of stimulus duration. Results for each subject (location) are shown on a different row (column). Results for small (large) cues are shown in black (red) lines. Posterior expectations and 95% credible intervals are estimated by MCMC.

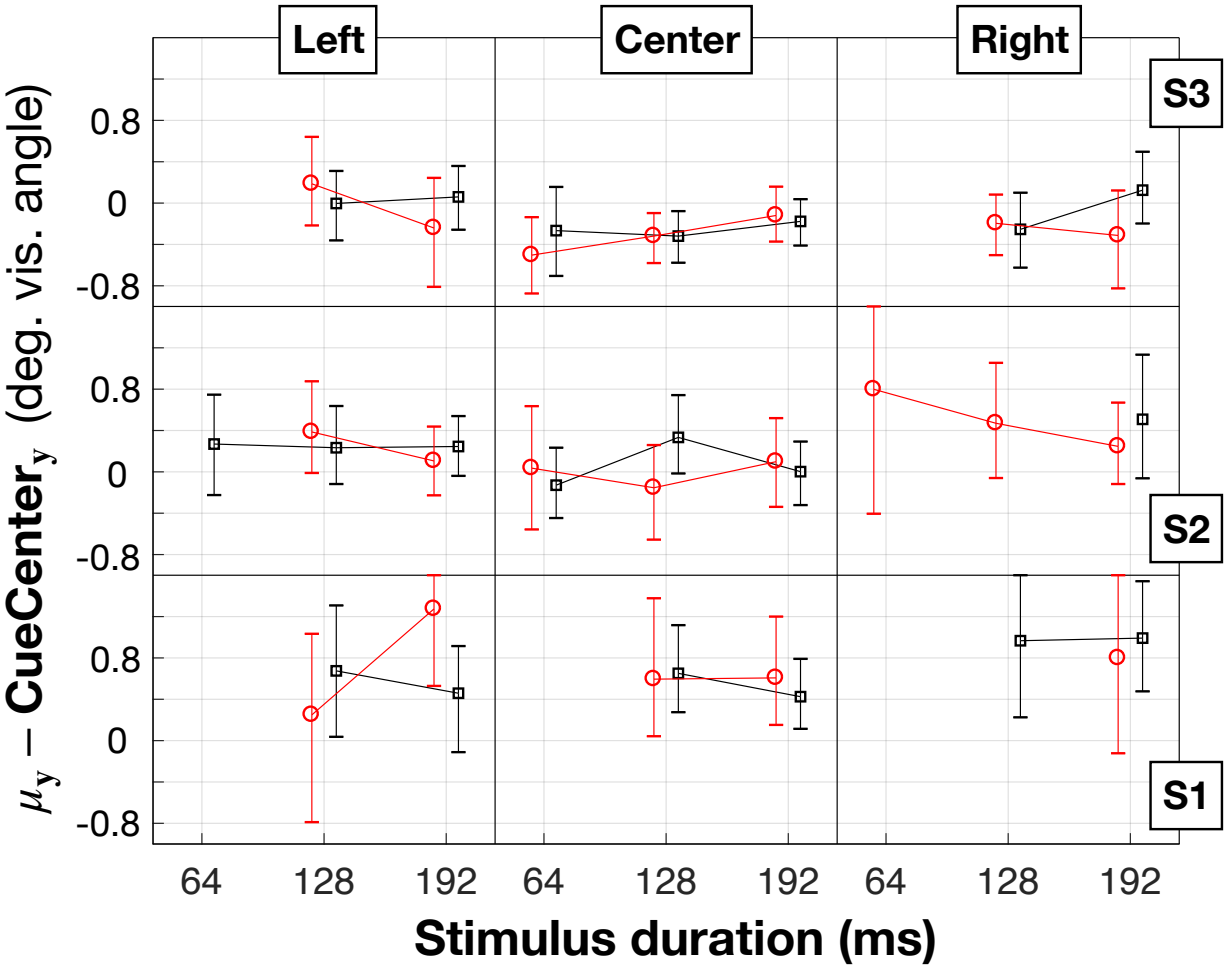

Figure 4.12: This figure shows how vertical deviations of the attentional locus vary across levels of stimulus duration. Results for each subject (location) are shown on a different row (column). Results for small (large) cues are shown in black (red) lines. Posterior expectations and 95% credible intervals are estimated by MCMC.

While some deviations appear significant, they are too small in magnitude to suggest subjects are systematically misdirecting their attentional spotlight to regions of space outside the cue.

4.5.4.4 Size of attentional spotlight

The product of scale parameters $\alpha_x \alpha_y$ is a measure of size. Using this measure, we can compare the rectangular area of the spotlight across conditions.

Figure 4.13 shows posterior expectations and 95% credible intervals for this transformation of model parameters in conditions where mean data-drivenness exceeds 1/2. All subjects appear to deploy a strategy attending to a region of space that is much smaller than the area of the cued region (*note*: small (large) cue area is 110.47 (178.60) degrees of visual angle squared). This result is visually apparent in top panels of figure 4.7.

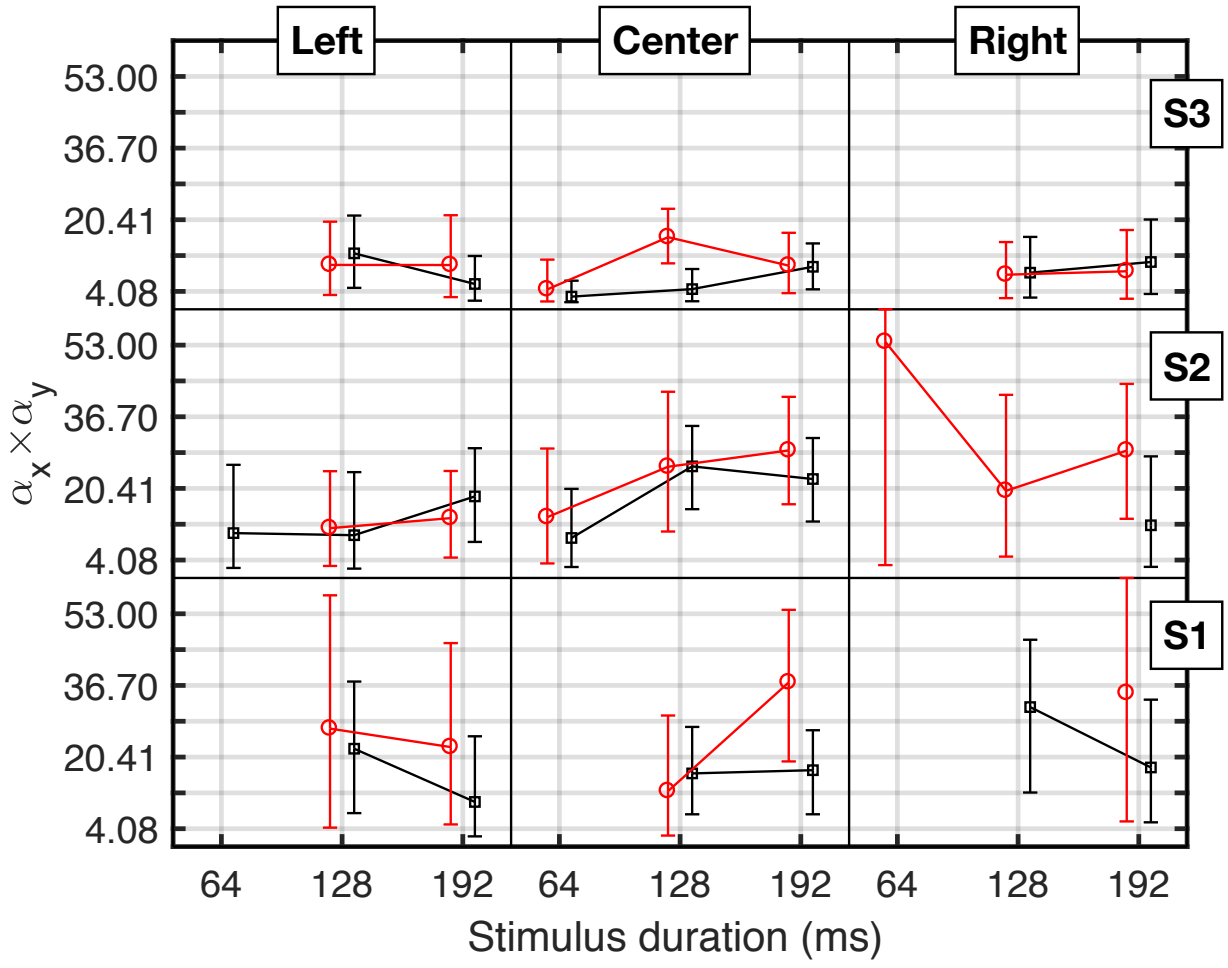

Figure 4.13: This figure shows how rectangular area of the attentional spotlight varies across levels of stimulus duration. Results for each subject (location) are shown on a different row (column). Results for small (large) cues are shown in black (red) lines. Posterior expectations and 95% credible intervals are estimated by MCMC.

While there is little-to-no evidence of cue size effects across subjects, subject 3 appears to show a location-by-duration dependent effect of cue size. For subject 3, the rectangular area

of the spotlight tends to increase with the size of the cue, but only when attending to the fovea and stimulus duration is 128 ms.

4.5.4.5 Shape of attentional spotlight

Symmetry

The ratio of scale parameters α_x/α_y is a measure of shape. Using this measure, we can compare the circular symmetry of the spotlight across conditions. When the value of this ratio is 1, the spotlight is circularly symmetric. For horizontally compressed spotlights, the value is less than 1. For vertically compressed spotlights, the value is greater than 1.

Figure 4.14 shows posterior expectations and 95% credible intervals for this transformation of model parameters in conditions where mean data-drivenness exceeds 1/2.

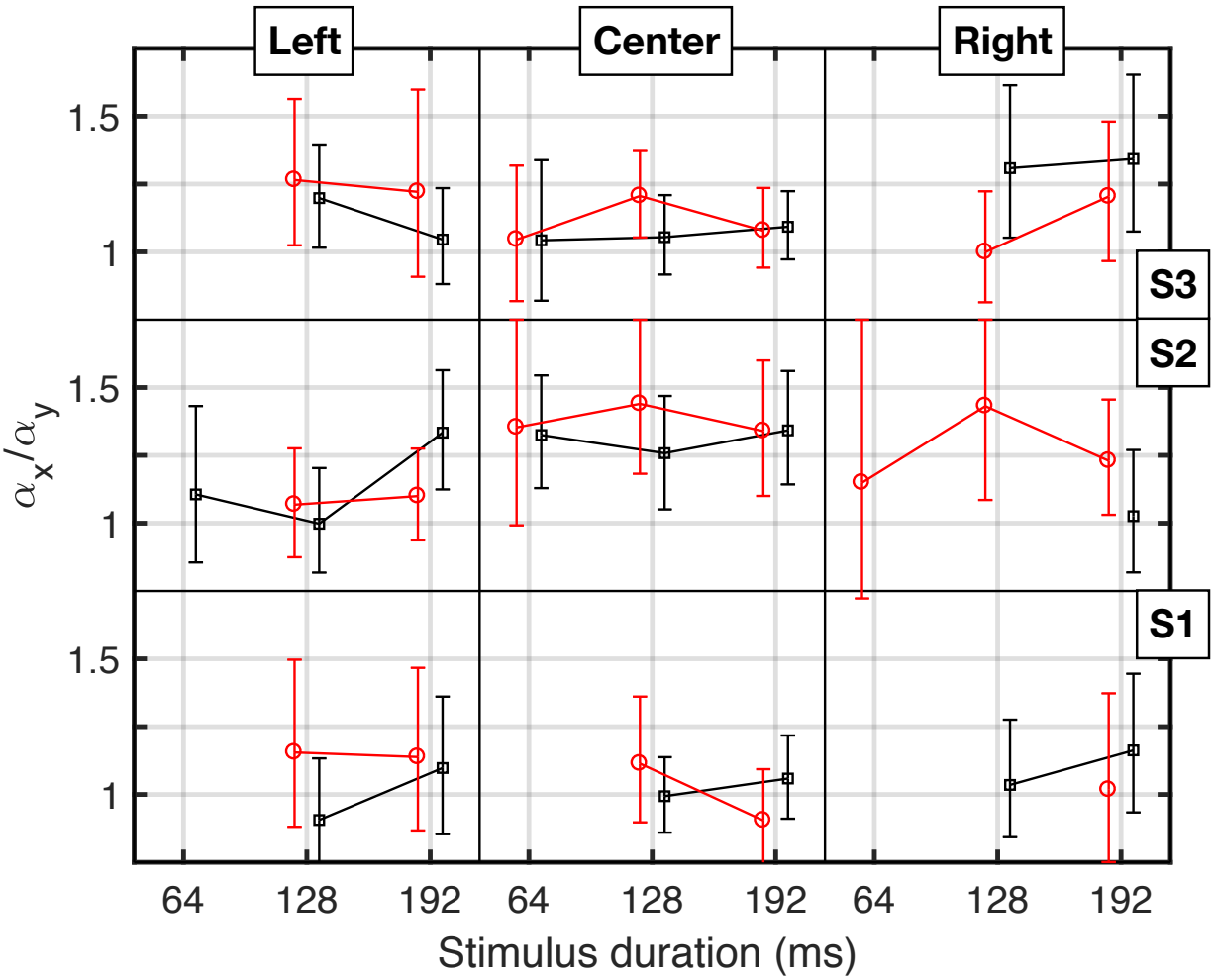

Figure 4.14: This figure shows how circular symmetry of the attentional spotlight varies across levels of stimulus duration. Results for each subject (location) are shown on a different row (column). Results for small (large) cues are shown in black (red) lines. Posterior expectations and 95% credible intervals are estimated by MCMC.

Subject 1 appears able to achieve a circularly symmetric spotlight in all experimental conditions.

Subjects 2 and 3 appear unable to achieve circularly symmetric spotlights under some experimental conditions. For subject 2, vertical compression is more apparent when attending to the fovea than the periphery. For subject 3, vertical compression is most apparent when attending to smaller cues located in the right periphery. There is also vertical compression in the left periphery for both cue sizes which appears alleviated by increasing stimulus duration.

Steepness

The gradient of 4.2 shows the ratio α_x/α_y does not provide a complete description of the shape of the spotlight because it neglects the contribution of κ. In order to provide a fuller description of shape, we introduce the following transformation of model parameters:

$$\frac{\kappa}{\sqrt{\alpha_x^2 + \alpha_y^2}} \tag{4.6}$$

Using this measure of shape, we can compare the steepness of the spotlight across experimental conditions.

Figure 4.15 shows posterior expectations and 95% credible intervals for this transformation of model parameters in conditions where mean data-drivenness exceeds 1/2.

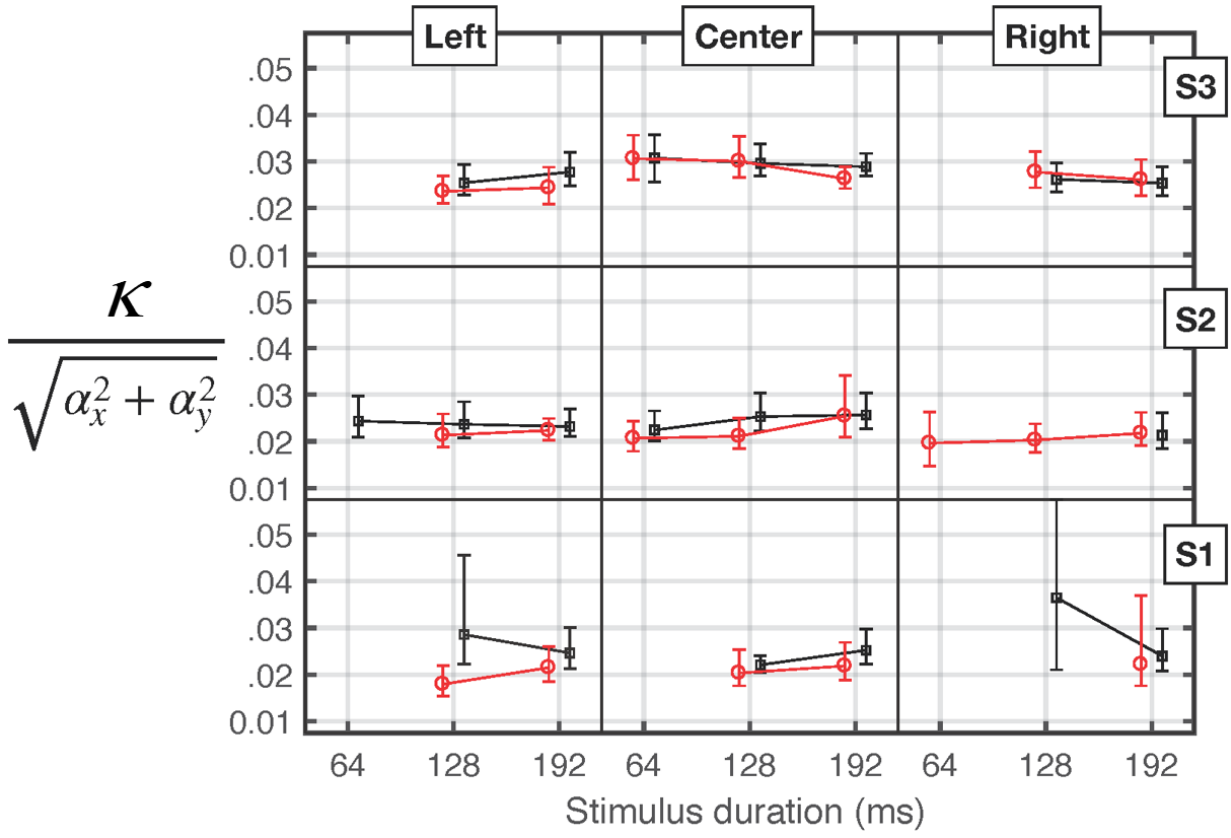

Figure 4.15: This figure shows how steepness of the attentional spotlight varies across levels of stimulus duration. Results for each subject (location) are shown on a different row (column). Results for small (large) cues are shown in black (red) lines. Posterior expectations and 95% credible intervals are estimated by MCMC.

Subjects 2 and 3 show little-to-no evidence that this measure of shape varies with the experimental factors. Interestingly, the posterior expectations for these two subjects are much more similar than those in figure 4.13.

Subject 1 shows a location-by-duration dependent effect of cue size. For subject 1, steepness of the spotlight tends to decrease when attending to larger regions, but only when attending to the left periphery and stimulus duration is 128 ms.

4.6 Discussion

In the current report, a total of 18 experimental conditions were presented in a factorial design with the levels of factors stimulus duration and cue size fixed for a given block of trials, and factor of cue location varying within the block. Thus, in any given block of trials, the spatial cue appeared centered on the fovea 1/3 of the time, in the left periphery 1/3 of the time, and in the right periphery 1/3 of the time. In every condition, a stimulus cloud of 42 dots was presented 768 milliseconds after the cue onset. Depending on the condition, the cloud persisted for 64, 128, or 192 milliseconds. Subjects were instructed to estimate the centroid (i.e. center of mass), restricted to dots positioned inside or on the boundary of the cue. The cursor for reporting the estimate appeared at the onset of the trial, and remained fixed in position at the center of the display until after the post-stimulus mask. When it was time to provide a response, the subject gained control over the cursor position via the mouse. Subjects were instructed to keep the cursor foveated at all times during the trial. In every condition, the optimal estimation strategy is to apply a filter to the stimulus that is uniform over the cued region, and zero everywhere else. The strategic-estimator modeling framework allows us to measure the distance between any subject's attentional spotlight and the optimal one (i.e. suboptimality). Then, given measurements of this distance taken

separately for each experimental condition, we can infer how differences in suboptimaltity are affected by variation in the factors of interest.

The kinds of effects and interactions we are able to detect heavily depend on subject-by-location, which suggests there are within-subject differences between strategies deployed in the fovea or periphery.

The fact that systematic error magnitudes tend to be larger than random error magnitudes means most of the estimation errors are caused by defects in the estimation strategy. For a given subject, these defects are more apparent in some conditions than others. Regardless of these trends or idiosyncrasies, as systematic bias magnitudes increase, so does the magnitude of random errors. This positive correlation between systematic and random error magnitudes is expected when trying to maximize circular hit probabilities, but not trying to minimize the error distance. Statistically speaking, the effect of estimation bias on feedback can be masked by lowering the precision of action. This means increasing the value of σ so that circular dispersion effectively cancels the component of bias outside the threshold for success. This kind of optimization is most likely to occur when the systematic errors are caused by obligatory biases, because the sources of bias cannot be removed without experience indicating changes in the effectiveness of the mechanisms deployed by the strategy. In other words, when presented with evidence for a failing strategy, subjects will maximize their chances of success by lowering the precision of action before abandoning the strategy altogether.

Without any information regarding dots in the stimulus, the distribution over target locations is a circular normal centered on the cue. Because of this, subjects can expect a reasonable amount of success from deploying a strategy involving sensory awareness of only the cued region. By design, the model in equation 4.3 can capture this strategy with parameters $w_0 = 1$, $x_0 = C_x$, and $y_0 = C_y$. The relative likelihood of data under this model compared to the full model offers a model-based test of this hypothesis (however, see the cautionary

remarks related to figure 3.14). Still there remains the possibility that performance is limited by the memory of the cued location. This hypothesis could be tested directly by introducing conditions where the cue and dots are displayed simultaneously.

In terms of the temporal properties of deployment, Shih and Sperling (2002) suggest an attention window is opened 150 ms after receiving the location cue, and remains open for at least 200 ms, during which time it admits information from all newly attended locations simultaneously. Other empirical estimates for the critical time (i.e. time required to fully deploy window) vary with task and experimental conditions, but are typically less than a second (Carrasco, 2011). Under the current design, previous research suggests our subjects have enough time to deploy their spotlights. If stimulus information were admitted from all attended locations simultaneously, we should not find an effect of stimulus duration. Instead, it appears the mechanism(s) of covert spatial attention do not admit information from all newly attended location simultaneously.

In the current design, we cannot rule out the possibility that changes in estimation strategy are driven by changes in noise-exclusion. However, we can rule out the possibility of signal enhancement because the dots were displayed at saturated contrast (Hetley et al., 2014). It would be possible to compare these two possibilities by lowering the stimulus contrast, and introducing an external noise factor into the current design.

4.6.1 Stimulus duration affects systematic, but not random, estimation error

The fact that the duration of stimulus information affects systematic error, but not random error, suggests the availability of dot information changes the effectiveness of mechanisms deployed by the estimation strategy. In the future, it would be useful to know whether the

systematic errors at shortest stimulus duration can be ameliorated with training; if not, then they may be explained by obligatory biases.

4.6.2 Random error is greater in large-cue vs. small-cue conditions

Changes in stimulus size influencing random error has been reported previously (Bingham and Muchisky, 1993a,b). The fact that changes cue size affects random error, but not systematic error, suggests changing the size of the attended region does not alleviate the defects in estimation strategy. Future investigations into these defects should choose small cue sizes because it makes systematic error components easier to detect.

4.6.3 Responses show higher data-drivenness at longer stimulus durations

According to the model, data-drivenness tends to increase with stimulus duration (see figure 4.9). In particular, data-drivenness tends to be higher at the shortest stimulus duration when subjects attend to the fovea than the periphery. This might explain some of the relationship between stimulus duration and systematic error in terms that are not related to the aspects of the spotlight captured by the model. For example, subject 1 appears to be systematically biased towards the anchor location (x_0, y_0) at shortest stimulus duration. Increasing the duration to 128 milliseconds alleviates this defect by for center and left conditions, but not the right.

4.6.4 Performance is better for center vs. left/right conditions

Recently, interest in peripheral vision has changed the way we think about visual attention operating in the periphery (Balas et al., 2009; Rosenholtz et al., 2012). Michel and Geisler (2011) note that for any task, the sources of uncertainty will always vary between foveal and peripheral vision. In those experiments, the data was explained by an ideal observer whose position estimates become less certain at greater retinal eccentricities. Wright et al. (2011) demonstrated that peripheral centroid estimation is not only biased towards the fovea, it is shifted towards the locus of attention by a separate mechanism. In those studies, model evidence suggests spatial attention is distributed as a function of retinal eccentricity. These sorts of effects have been predicted by models of attention shifting the receptive fields of cortical neurons (Baruch and Yeshurun, 2014).

The current study provides evidence that a given subject deploys different strategies to the fovea and periphery. This evidence comes in the form of interaction effects. For example, subject 2 in figure 4.9 appears to not use an anchoring point when attending to the fovea, regardless of the stimulus duration. In fact, for all subjects, data-drivenness tends to be higher at the shortest stimulus duration when subjects attend to the fovea. This suggests covert spatial attention has a larger effect on the temporal resolution of the fovea than the periphery.

According to the current model, suboptimality tends to decrease with stimulus duration when attending to the fovea (see figure 4.8). This might explain some of the relationship between stimulus duration and systematic error in terms that are related to the aspects of the spotlight captured by the model. Unlike biases explained by low data-drivenness, the directions/magnitudes of bias explained by defects of the spotlight will depend on properties of the stimulus encoded by the mechanisms responsible for the bias.

4.6.5 Performance in left/right conditions varies idiosyncratically across subjects

Many subjects show evidence of peripheral asymmetries. This suggests a given subject may not deploy the same strategy to all areas of the periphery. For example, in figure 4.9, subject 2 shows an effect of cue size on the right (but not the left) periphery. According to the figure, this subject deploys a strategy to the right periphery that is more data-driven for large cue conditions. For another example, in figure 4.14, subject 3 shows a possible interaction between cue size and peripheral location. According to the figure, this subject deploys a spotlight to the right (left) periphery than is asymmetric for small (large) cue conditions, but not large (small) cue conditions.

4.6.6 Subjects show little flexibility in the sizes and shapes of spotlights they can achieve

Previous models of spatial attention have described a "spotlight" of fixed size and shape that can be deployed anywhere in the visual field to facilitate processing under the spotlight at the cost of processing elsewhere (Posner, 1980). Alternative descriptions allow some flexibility in the size and shape of the spotlight, but claim larger windows are limited to smaller amplitudes (i.e. weaker signal), which limits performance (Eriksen and James, 1986). Other limitations due to the spatial resolution have been measured experimentally (Gobell et al., 2004).

Figures 4.13, 4.14, 4.15 show that while much of the systematic error can be attributed to mismatches between the optimal and achieved spotlights, subjects do not change their strategy in ways that are easy to detect with these measures. In contrast, figures 4.11 and 4.12 show that subjects do make changes to the location of the spotlight depending on

the location of the cue. In most cases, the credible intervals include 0, which suggests the subjects are orienting correctly. In exceptional cases, the deviations are small enough in magnitude that mismatches between the optimal and achieved spotlights are rarely, if ever, due to misdirection of the attentional locus.

Taken together, the results in figures 4.14 and 4.15 suggest subjects choose from a set of strategies with little-to-no flexibility over the shape of the spotlight. Combined with the results in figures 4.11 and 4.12, if spatial attention operates like a spotlight, then it seems subjects are flexible in choosing where to direct the spotlight, but not in the size or shape of the illuminated region.

4.6.7 Regardless of size or shape, spotlights are approximately Gaussian or exponential

Figure 4.10 shows with rare exceptions, it appears all subjects deploy a spotlight with volume distributed much like the normal distribution. In the exceptional cases, the volume is distributed with higher-than-normal kurtosis, indicating an exponential decay. These exceptional cases do not appear systematically related to the experimental condition, which suggests subjects have little-to-no flexibility in this aspect of their strategy.

The regularity of this result across subjects might explain why figure 4.15 shows much less evidence of individual differences than one might expect based on the information in figures 4.7 or 4.13. Individual differences in size are detectable when it is measured with rectangular area or the denominator of equation 4.6, but much less apparent in figure 4.15. This result may be useful for future investigations trying to find a better measure of shape than the ones we used here.

4.6.8 Implications for psychophysical investigations and neuro-computational models of visual attention

(Sun et al., 2013) provides an inference framework for studying feature-based attention with centroid tasks. The work in this chapter attempts to provide an inference framework for spatial attention. In our design, distractor items are dots not located inside or on the boundary of the cue. Previous psychophysical investigations into the mechanism(s) of visual attention are dominated by visual search tasks, which inherently confound the mechanisms of spatial and feature-based attention. Visual search tasks have been used to study and compare feature-based and spatial attention (Kim and Cave, 1995; Eckstein et al., 2000; Moore and Egeth, 1998; Shih and Sperling, 1996). In the typical visual search experiment, subjects are presented with variable-sized arrays that may or may not contain the target item. The task is to use knowledge of the target's position or features to facilitate detection whenever the target is present. The general finding is that adding non-target objects into a display will increase reaction times and error rates (Wolfe, 1998). However, advanced knowledge about a target's position will reduce the impact of non-targets at different positions (Eckstein, 2011). According to signal detection theory, increasing the number of distractors impairs performance because of greater uncertainty over which locations provide information about the target and not distractors. This effect is ameliorated by cues to spatial attention because they allow noise-filtering over events registered at locations where distractors are most likely to occur (Eckstein et al., 2009).

Convergent evidence from neural recording and perceptual phenomena indicate spatial attention modulates early sensory representations at the level of individual neurons, and the effect(s) of these early modulations propagate forward to influence perceptual representation of visual objects (Luck et al., 1997; McAdams and Maunsell, 1999; Cameron et al., 2002). These influences can be measured psychophysically, and explain performance-related changes in visual acuity (Shiu and Pashler, 1995), contrast- and orientation- thresholds (Lee et al.,

1997; Prinzmetal et al., 1998), and localization (Tsal and Bareket, 1999). This might explain why our subjects are limited to strategies involving spotlights that are approximately Gaussian or exponential, if the neurons recruited for a given strategy have approximately Gaussian or exponential receptive fields. Competition for neural resources may be biased towards locations where targets are most likely to appear (Moran and Desimone, 1985). This would explain the flexibility of spotlight locations and apparent Gaussianity of spotlight shapes, in terms of biased competition for resources required to decode signals from neurons with approximately Gaussian receptive fields.

(David et al., 2008) reported different effects of spatial and feature-based attention on neural response of V4 during visual search tasks. Spatial attention seems to modulate response baseline and gain, but not tuning for orientation or spatial frequency. In contrast, feature-based attention can modify tuning– which increases sensitivity to the features that distinguish the target from distractors (Elder and Zucker, 1993). This difference is consistent with the differences in selectivity we see in the current experiment and those designed to study feature-based attention. If the mechanism of heightened selectivity was a shift in neural tuning, then we expect comparable selectivity ratios between centroid tasks where targets are delineated from distractors by a boundary. Contrary to this prediction, we conjecture selectivity ratios are higher for boundaries in feature space, compared to boundaries in visual space. Accordingly, this suggests the reason subjects are better at selecting subsets of feature space vs. visual space is related to shifts of neural tuning improving feature discriminability, but not spatial acuity.

Bibliography

Attneave, F. (1954). Some informational aspects of visual perception. *Psychological review*, 61(3):183.

Badcock, D. R., Hess, R. F., and Dobbins, K. (1996). Localization of element clusters: Multiple cues. *Vision Research*, 36(10):1467–1472.

Balas, B., Nakano, L., and Rosenholtz, R. (2009). A summary-statistic representation in peripheral vision explains visual crowding. *Journal of vision*, 9(12):13–13.

Baruch, O. and Yeshurun, Y. (2014). Attentional attraction of receptive fields can explain spatial and temporal effects of attention. *Visual Cognition*, 22(5):704–736.

Baud-Bovy, G. and Soechting, J. (2001). Visual localization of the centre of mass of compact, asymmetric, two-dimensional shapes. *Journal of Experimental Psychology: Human Perception and Performance*, 27:692–706.

Bingham, G. P. and Muchisky, M. M. (1993a). Center of mass perception and inertial frames of reference. *Perception & Psychophysics*, 54(5):617–632.

Bingham, G. P. and Muchisky, M. M. (1993b). Center of mass perception: Perturbation of symmetry. *Perception & Psychophysics*, 54(5):633–639.

Bock, M. E. and Solomon, H. (1988). Distributions of quadratic forms. *Australian Journal of Statistics*, 30(1):139–149.

Brainard, D. H. (1997). The psychophysics toolbox. *Spatial Vision*, 10:433–436.

Cameron, E. L., Tai, J. C., and Carrasco, M. (2002). Covert attention affects the psychometric function of contrast sensitivity. *Vision research*, 42(8):949–967.

Carrasco, M. (2011). Visual attention: The past 25 years. *Vision Research*, 49(10):1484–1525.

Casella, G. and Berger, R. L. (2002). *Statistical inference*, volume 2. Duxbury Pacific Grove, CA.

Cholewiak, S. A., Fleming, R. W., and Singh, M. (2015). Perception of physical stability and center of mass of 3-d objects. *Journal of vision*, 15(2):13–13.

Chubb, C., Landy, M. S., and Econopouly, J. (2004). A visual mechanism tuned to black. *Vision research*, 44(27):3223–3232.

Cochran, W. G. (1934). The distribution of quadratic forms in a normal system, with applications to the analysis of covariance. In *Mathematical Proceedings of the Cambridge Philosophical Society*, volume 30, pages 178–191. Cambridge University Press.

Craft, E., Schutze, H., Niebur, E., and von der Heydt, R. (2007). A neural model of figure–ground organization. *Journal of neurophysiology*, 97(6):4310–4326.

Crajé, C., Santello, M., and Gordon, A. M. (2013). Effects of visual cues of object density on perception and anticipatory control of dexterous manipulation. *PloS one*, 8(10):e76855.

Davi, M., Doyle, M. A. T., and Proffitt, D. R. (1992). The role of symmetry in determining perceived centers within shapes. *Perception & psychophysics*, 52(2):151–160.

David, S. V., Hayden, B. Y., and Gallant, J. L. (2006). Spectral receptive field properties explain shape selectivity in area v4. *Journal of neurophysiology*, 96(6):3492–3505.

David, S. V., Hayden, B. Y., Mazer, J. A., and Gallant, J. L. (2008). Attention to stimulus features shifts spectral tuning of v4 neurons during natural vision. *Neuron*, 59(3):509–521.

Drew, S., Chubb, C., and Sperling, G. (2010). Precise attention filters for weber contrast derived from centroid estimations. *Journal of Vision*, 10(10:20):1–16, http://www.journalofvision.org/content/10/10/20.

Driver, J. and Baylis, G. C. (1989). Movement and visual attention: the spotlight metaphor breaks down. *Journal of Experimental Psychology: Human perception and performance*, 15(3):448.

Eckstein, M. P. (2011). Visual search: A retrospective. *Journal of vision*, 11(5):14–14.

Eckstein, M. P., Peterson, M. F., Pham, B. T., and Droll, J. A. (2009). Statistical decision theory to relate neurons to behavior in the study of covert visual attention. *Vision research*, 49(10):1097–1128.

Eckstein, M. P., Thomas, J. P., Palmer, J., and Shimozaki, S. S. (2000). A signal detection model predicts the effects of set size on visual search accuracy for feature, conjunction, triple conjunction, and disjunction displays. *Perception & psychophysics*, 62(3):425–451.

Elder, J. and Zucker, S. (1993). The effect of contour closure on the rapid discrimination of two-dimensional shapes. *Vision Research*, 33(7):981–991.

Eriksen, B. A. and Eriksen, C. W. (1974). Effects of noise letters upon the identification of a target letter in a nonsearch task. *Perception & psychophysics*, 16(1):143–149.

Eriksen, C. W. and James, J. D. S. (1986). Visual attention within and around the field of focal attention: A zoom lens model. *Perception & psychophysics*, 40(4):225–240.

Feldman, J. and Singh, M. (2005). Information along contours and object boundaries. *Psychological review*, 112(1):243.

Field, D. J., Hayes, A., and Hess, R. F. (1993). Contour integration by the human visual system: evidence for a local "association field". *Vision research*, 33(2):173–193.

Fraser, D. (1953). Generalized hit probabilities with a gaussian target, ii. *The Annals of Mathematical Statistics*, pages 288–294.

Fraser, D. A. S. et al. (1951). Generalized hit probabilities with a gaussian target. *The Annals of Mathematical Statistics*, 22(2):248–255.

Gobell, J., Tseng, C.-H., and Sperling, G. (2004). The spatial distribution of visual attention. *Vision Research*, 44:1273–1296.

Golla, H., Ignashchenkova, A., Haarmeier, T., and Thier, P. (2004). Improvement of visual acuity by spatial cueing: A comparative study in human and non-human primates. *Vision research*, 44(13):1589–1600.

Grad, A. and Solomon, H. (1955). Distribution of quadratic forms and some applications. *The Annals of Mathematical Statistics*, pages 464–477.

Harter, H. L. (1960). Circular error probabilities. *Journal of the American Statistical Association*, 55(292):723–731.

He, P. and Kowler, E. (1989). The role of location probability in the programming of saccades: Implications for "center-of-gravity" tendencies. *Vision research*, 29(9):1165–1181.

Hess, R., Hayes, A., and Field, D. (2003). Contour integration and cortical processing. *Journal of Physiology-Paris*, 97(2-3):105–119.

Hess, R. F., Dakin, S. R., and Badcock, D. (1994). Localization of element clusters by the human visual system. *Vision Research*, 34(18):2439–2451.

Hetley, R., Dosher, B. A., and Lu, Z.-L. (2014). Generating a taxonomy of spatially cued attention for visual discrimination: effects of judgment precision and set size on attention. *Attention, Perception, & Psychophysics*, 76(8):2286–2304.

Izhikevich, E. M. (2007). *Dynamical systems in neuroscience*. MIT press.

Kim, M.-S. and Cave, K. R. (1995). Spatial attention in visual search for features and feature conjunctions. *Psychological Science*, 6(6):376–380.

Konen, C. S. and Kastner, S. (2008). Two hierarchically organized neural systems for object information in human visual cortex. *Nature neuroscience*, 11(2):224.

Kovács, I., Fehér, A., and Julesz, B. (1998). Medial-point description of shape: a representation for action coding and its psychophysical correlates. *Vision research*, 38(15-16):2323–2333.

Kowler, E., Anderson, E., Dosher, B., and Blaser, E. (1995). The role of attention in the programming of saccades. *Vision research*, 35(13):1897–1916.

Kowler, E. and Blaser, E. (1995). The accuracy and precision of saccades to small and large targets. *Vision research*, 35(12):1741–1754.

Lee, D. K., Koch, C., and Braun, J. (1997). Spatial vision thresholds in the near absence of attention. *Vision research*, 37(17):2409–2418.

Lehky, S. R. and Sereno, A. B. (2007). Comparison of shape encoding in primate dorsal and ventral visual pathways. *Journal of neurophysiology*, 97(1):307–319.

Luck, S. J., Chelazzi, L., Hillyard, S. A., and Desimone, R. (1997). Neural mechanisms of spatial selective attention in areas v1, v2, and v4 of macaque visual cortex. *Journal of neurophysiology*, 77(1):24–42.

McAdams, C. J. and Maunsell, J. H. (1999). Effects of attention on orientation-tuning functions of single neurons in macaque cortical area v4. *Journal of Neuroscience*, 19(1):431–441.

McGowan, J. W., Kowler, E., Sharma, A., and Chubb, C. (1998). Saccadic localization of random dot targets. *Vision Research*, 38:895 – 909.

Michel, M. and Geisler, W. S. (2011). Intrinsic position uncertainty explains detection and localization performance in peripheral vision. *Journal of Vision*, 11(1):18–18.

Moore, C. M. and Egeth, H. (1998). How does feature-based attention affect visual processing? *Journal of Experimental Psychology: Human Perception and Performance*, 24(4):1296.

Moran, J. and Desimone, R. (1985). Selective attention gates visual processing in the extrastriate cortex. *Science*, 229(4715):782–784.

Moreland, J. C. and Boynton, G. M. (2017). A neurophysiological explanation for biases in visual localization. *Attention, Perception and Psychophysics*, 79:553–562.

Newton, I. (1999). *The Principia: mathematical principles of natural philosophy*. Univ of California Press.

Norman, D. A. (1968). Toward a theory of memory and attention. *Psychological review*, 75(6):522.

Pasupathy, A. and Connor, C. E. (2002). Population coding of shape in area v4. *Nature neuroscience*, 5(12):1332.

Posner, M. I. (1980). Orienting of attention. *Quarterly journal of experimental psychology*, 32(1):3–25.

Prinzmetal, W., Amiri, H., Allen, K., and Edwards, T. (1998). Phenomenology of attention: I. color, location, orientation, and spatial frequency. *Journal of Experimental Psychology: Human Perception and Performance*, 24(1):261.

Proffitt, D. R., Thomas, M. A., and O'Brien, R. G. (1983). The roles of contour and luminance distribution in determining perceived centers within shapes. *Perception and Psychophysics*, 33(1):63–71.

Qiu, F. T., Sugihara, T., and Von Der Heydt, R. (2007). Figure-ground mechanisms provide structure for selective attention. *Nature neuroscience*, 10(11):1492.

Ratcliff, R., Voskuilen, C., and McKoon, G. (2018). Internal and external sources of variability in perceptual decision-making. *Psychological review*, 125(1):33.

Reeves, A. and Sperling, G. (1986). Attention gating in short-term visual memory. *Psychological review*, 93(2):180.

Robson, J. G. (1980). Neural images: The physiological basis of spatial vision. In Harris, C. S., editor, *Visual Coding and Adaptability*, pages 177–214. Erlbaum, Hillsdale, NJ.

Roelfsema, P. R., Lamme, V. A., and Spekreijse, H. (1998). Object-based attention in the primary visual cortex of the macaque monkey. *Nature*, 395(6700):376.

Roelfsema, P. R., Lamme, V. A., Spekreijse, H., and Bosch, H. (2002). Figure—ground segregation in a recurrent network architecture. *Journal of cognitive neuroscience*, 14(4):525–537.

Rosenholtz, R., Huang, J., Raj, A., Balas, B. J., and Ilie, L. (2012). A summary statistic representation in peripheral vision explains visual search. *Journal of Vision*, 12(4:14):1–17.

Sereno, A. B. and Maunsell, J. H. (1998). Shape selectivity in primate lateral intraparietal cortex. *Nature*, 395(6701):500.

Shih, S.-I. and Sperling, G. (1996). Is there feature-based attentional selection in visual search? *Journal of Experimental Psychology: Human Perception and Performance*, 22(3):758.

Shih, S.-I. and Sperling, G. (2002). Measuring and modeling the trajectory of visual spatial attention. *Psychological review*, 109(2):260.

Shiu, L.-P. and Pashler, H. (1995). Spatial attention and vernier acuity. *Vision Research*, 35(3):337–343.

Sigurdardottir, H. M., Michalak, S. M., and Sheinberg, D. L. (2014). Shape beyond recognition: Form-derived directionality and its effects on visual attention and motion perception. *Journal of Experimental Psychology: General*, 143(1):434.

Solomon, H. (1953). Distribution of the measure of a random two-dimensional set. *The Annals of Mathematical Statistics*, pages 650–656.

Solomon, H. et al. (1961). On the distribution of quadratic forms in normal variates. In *Proceedings of the Fourth Berkeley Symposium on Mathematical Statistics and Probability, Volume 1: Contributions to the Theory of Statistics*. The Regents of the University of California.

Sperling, G. (2008). Type i and type ii experiments.

Sun, P., Herrera, C., Chubb, C., Wright, C. E., and Sperling, G. (2013). Attention filters for colors: isolating single colors. *Journal of Vision*, page forthcoming (abstract).

Tsal, Y. and Bareket, T. (1999). Effects of attention on localization of stimuli in the visual field. *Psychonomic Bulletin & Review*, 6(2):292–296.

Tschechne, S. and Neumann, H. (2014). Hierarchical representation of shapes in visual cortex—from localized features to figural shape segregation. *Frontiers in computational neuroscience*, 8:93.

Von der Heydt, R., Peterhans, E., and Baumgartner, G. (1984). Illusory contours and cortical neuron responses. *Science*, 224(4654):1260–1262.

Vos, P. G., Bocheva, N., Yakimoff, N., and Helsper, E. (1993). Perceived location of two-dimensional patterns. *Vision Research*, 33(15):2157–2169.

Wagenmakers, E.-J., Lodewyckx, T., Kuriyal, H., and Grasman, R. (2010). Bayesian hypothesis testing for psychologists: A tutorial on the savage–dickey method. *Cognitive psychology*, 60(3):158–189.

Washburn, A. R., Kress, M., et al. (2009). *Combat modeling*, volume 139. Springer.

Wilks, S. S. (1944). *Mathematical Statistics*. Princeton University Press.

Wolfe, J. M. (1998). What can 1 million trials tell us about visual search? *Psychological Science*, 9(1):33–39.

Wright, J. M., Morris, A. P., and Krekelberg, B. (2011). Weighted integration of visual position information. *Journal of Vision*, 11(14):11–11.